On Symmetric Stability and Instability of Zonal Mean Flows Near the Equator

by
Duane E. Stevens

Department of Atmospheric Science
Colorado State University
Fort Collins, Colorado

Colorado State University

Department of Atmospheric Science

Paper No. 356

ON SYMMETRIC STABILITY AND INSTABILITY OF ZONAL MEAN FLOWS NEAR THE EQUATOR

Duane E. Stevens

Department of Atmospheric Science

Colorado State University

Fort Collins, CO 80523

September 1982

Atmospheric Science Paper No. 356

Abstract

Observations of longitudinally-averaged zonal flows in the atmosphere and ocean tend to display north-south symmetry about the equator, with a characteristic wind maximum or minimum and therefore little horizontal wind shear locally near the equator. It is shown that this configuration is required for balanced flow on a sphere to be inertially stable. Any horizontal wind shear at the equator will cause a symmetric instability to develop, effectively eliminating the horizontal shear. It follows that the potential vorticity must vanish at the equator. Balanced cross-equatorial flow can occur only if there is a north-south gradient in the torque or the diabatic heating at the equator. These conclusions are obtained under the assumption of a balanced zonal flow; i.e., acceleration and dissipation are explicitly neglected in the meridional momentum equation.

The characteristics of the equatorial symmetric instability that develops if the mean flow is horizontally sheared at the equator are investigated. The analysis with Rayleigh friction and Newtonian cooling follows and extends the brief treatment of inviscid instability on the equatorial beta-plane by Dunkerton (1981). Quadratic as well as linear shear is considered.

If only real values of the separation constant (equivalent depth h) are considered, so that vertical wavenumber is real, Dunkerton's results are reproduced. The instability is confined to the region in which the vertical component of absolute vorticity is of opposite sign to the local Coriolis parameter; i.e., where the square of the inertial frequency is negative. The mode of greatest instability is a meridional overturning with a single cell in the horizontal dimension which tends

to mix angular momentum, thereby eliminating the horizontal gradient of angular momentum at the equator. With this particularly simple parameterization of mechanical and thermal dissipation, the mixing occurs most readily at the smallest vertical scales and the gravest (n = 0) meridional mode. When the flow curvature is much less than β, the maximum growth rate for symmetric instability is approximately one-half the magnitude of the relative vorticity of the mean flow at the equator minus the mechanical dissipation rate. Hence the horizontal shear at the equator must exceed twice the Rayleigh friction coefficient for instability. Thermal dissipation does not affect the instability criterion.

If complex equivalent depths are considered, these conclusions are radically altered. We confine our attention to those eigenmodes that are bounded on the horizontally infinite equatorial beta-plane and bounded with height. In addition, we require the unstable eigenfunctions to be limited to a pre-assigned horizontal length scale L which is defined by the shear region. Depending on the length scale L, the maximum instability can now occur at a finite rather than infinitesimal vertical scale. Modes with n>0 can now be more unstable than the n = 0 mode. With $L \gtrsim 500$ km, greatest instability occurs when the real and imaginary parts of $\sqrt{gh}$ are the same order of magnitude. The (inviscid) growth rate can now exceed the shear. The eigensolutions are trapped vertically and exhibit poleward and downward phase propagation.

Many recent studies have been undertaken which investigate the effect of mean zonal flow on tropical waves and instabilities. A consequence of the present analysis is that a stationary, non-dissipative basic state flow with horizontal shear at the equator is inappropriate

because it is not a stable solution of the symmetric governing equations. This instability tends to symmetrize the zonal flow with respect to the equator if mechanical dissipation is not too great. It also provides a possible theoretical mechanism for the symmetric component of the 40-50 day oscillation in the tropical atmosphere. While Dunkerton (1981) focused on the ramifications for the middle atmosphere, this study applies the results primarily to tropospheric and oceanic circulations.

Acknowledgments

It is a pleasure to acknowledge many fruitful discussions with several colleagues in the Department of Atmospheric Science at Colorado State University. I am grateful to John Anderson (CSU) for pointing out the application of this analysis to the 40-50 day oscillation. In addition, comments by Drs. John Boyd, Tim Dunkerton, Lloyd Shapiro, and an anonymous reviewer were very beneficial in improving the manuscript. The excellent skills of Machel Sandfort in word processing, Duayne Barnhart in photographing, and Hanae Akari and Judy Sorbie in drafting are much appreciated. The work was supported by NSF Grant ATM-8107136.

This paper has been submitted to the Journal of the Atmospheric Sciences for publication.

Table of Contents

1. Introduction

In seeking to understand the dynamical causes and properties of disturbances in a geophysical fluid, a common theoretical methodology is to investigate small-amplitude, linearized perturbations in the context of a zonally and temporally averaged basic state. It is generally assumed that this basic state circulation is a solution to the governing equations. In instability studies, the stability of a flow configuration is investigated to determine whether small-amplitude perturbations can spontaneously grow, gaining energy from the mean flow. Charney (1973) documents and classifies many types of hydrodynamic instability with applicability to geophysical fluids. Barotropic and baroclinic instabilities are important types of non-axisymmetric (three-dimensional) instabilities. As often conceptualized, axisymmetric (two-dimensional) disturbances result from inertial instability of a symmetric flow. Dunkerton (1982b) has recently discussed inertial (or centrifugal) instability as a mechanism for forcing nonsymmetric disturbances as well.

For studies of neutrally propagating waves, the basic state flow is generally assumed to be stationary in time. Implicitly, the flow must be stable, at least on the relevant time scale of the wave.

In the tropical atmosphere and ocean, one finds a tendency for the axisymmetric component of the circulation to exhibit north-south symmetry about the equator; i.e., the zonal flow tends to have a relative minimum or maximum at the equator, and the horizontal shear therefore vanishes locally. Figure 1 shows the observed mean zonal flow at 2-month intervals in 1957 and 1958, adapted from Fig. 10.24 of Newell et al. (1974). Within the limits of data accuracy, the horizontal shear of

the flow tends to vanish somewhere near the equator. This characteristic continues in the additional months of data in Newell et al. (not shown). There are of course significant non-axisymmetric components of the forcing (e.g., land-sea contrasts) and the circulation itself which affect the mean zonal flow through non-linear interactions; they are neglected in the present study. Figure 2 displays a section of zonal flow and temperature at a particular longitude and month in the Pacific Ocean. Again the tendency for currents to be centered on the equator is observed. The temperature is largely in thermal wind balance with the zonal flow.

The purpose of this study is to show that this configuration is not accidental. Rather, it is demonstrated that, with sufficiently small dissipation, any horizontal shear of the zonal flow at the equator causes a symmetric overturning by giving rise to inertial instability. The instability acts to restore the north-south symmetry of the flow by mixing the angular momentum horizontally, causing the north-south gradient of angular momentum to vanish locally at the equator.

In Section 2 we consider balanced symmetric flow on a sphere, obtaining conditions for the stability of such a flow. Section 3 addresses the characteristics of the symmetric instability when the flow is sheared locally at the equator. In Section 4 the applicability and some implications of the analysis are presented.

Dunkerton (1982) first addressed the equatorial shear problem on an equatorial beta plane, discovering that the flow is unstable for any magnitude of the shear if dissipation is neglected. In order to eliminate the shortest vertical scale as the most unstable mode, he introduced two forms of mechanical dissipation: second-order diffusion with an eddy viscosity and infinite-order diffusion.

A major conclusion of this paper is that his inviscid results were severely limited by the assumption of real equivalent depths. In Section 3c, we find modes of greater instability if complex equivalent depths are considered.

In this study, mechanical dissipation is parameterized as Rayleigh friction and thermal dissipation as Newtonian cooling. Although simpler than Dunkerton's method, the author believes this approach is certainly competitive, and perhaps superior. With the spatial scale-independent parameterization of dissipation, the dissipative time scales are the only free parameters and the present results do not depend crucially on the parameterization or the assumed coefficients. As Dunkerton essentially admitted in his Section 3d, second- and higher-order diffusion is an ad hoc parameterization which has not been proved superior by observations. Dunkerton did not provide physical justification for its use or for the magnitude of the diffusion coefficients; rather it would appear that it was applied because it gave the desired (aesthetic?) effect, a finite scale selection. He also pointed out that the turbulence may result from the inertial instability, causing the linear diffusion parameterization to break down.

Even more serious is the possibility that the diffusion results are inconsistent. Dunkerton took an inviscid result and proceeded with very little explanation to change the complex frequency (ω in his notation) to a diffusion-altered value, $\omega - i\nu m^2$, where ν is the eddy viscosity coefficient and m the vertical wavenumber. It may be argued that this is consistent locally, in the spirit of a small-number expansion. However, it is apparent that such a method does not yield a consistent global solution. Clearly, the problem formulation with second-order

diffusion is not separable in its horizontal and vertical dependence; yet a separated solution with a meridional mode number and vertical wave number is proposed. In addition, although a viscous eigensolution is proposed, the vertical wavenumber in his critical stability criterion (2.6) is assumed to result from an inviscid separation relationship with only real values. In an extension of this study, the author is investigating the instability criteria and growth rates without this last assumption.

Finally, it should be mentioned that other instabilities can certainly co-exist with the symmetric inertial instability. For example, (non-axisymmetric) barotropic and baroclinic instabilities may be important for a particular flow regime. Boyd and Christidis (1982) and Dunkerton (1982b) have recently emphasized nonsymmetric instabilities near the equator. They may even have faster growth rates. The point of this study is that symmetric inertial instability may also be possible and relevant in geophysical circulations near the equator. By assuming only two-dimensional perturbations, all nonsymmetric instabilities have been artificially suppressed. The beta-plane formulation of Section 3 also eliminates baroclinic and barotropic instabilities by assuming a zonal flow with only meridional shear which does not satisfy the necessary condition for barotropic instability, $\beta - \partial^2\bar{u}/\partial y^2 = 0$, anywhere in the domain.

2. Symmetric Stability on a Sphere

The condition for inertial stability of an incompressible fluid rotating in an azimuthally symmetric vortex on an f-plane has been well-documented (e.g., Eliassen, 1952; Shapiro and Willoughby, 1982; Schubert and Hack, 1982). With R denoting the radial distance from the local rotation axis, f twice the local rotation rate, U the aximuthal velocity component, $\zeta = \partial(RU)/R\partial R$ the relative vorticity, and $M = \frac{1}{2}fR^2 + RU$ the absolute angular momentum, Charney (1973) writes the stability criterion in the form

$$\sigma_I^2 = \frac{1}{R^3}\frac{\partial M^2}{\partial R} = (f + \frac{2U}{R})(f + \zeta) > 0. \tag{2.1}$$

σ_I is the frequency of inertial oscillation for a stable perturbation. If σ_I is imaginary, its magnitude gives the growth rate of an unstable disturbance. On a sphere, we shall find that an analogous relationship holds, with a latitudinal gradient replacing the radial gradient.

a. Mathematical development

In this section we develop the equations which govern a "balanced" zonally symmetric circulation on a sphere. Let us assume a flow in which the meridional pressure gradient balances the Coriolis and centrifugal terms in the meridional momentum equation. Meridional accelerations are neglected. This assumption causes the zonal flow to be analogous to the symmetric tangential wind in a balanced hurricane model (Ooyama, 1969). Assuming a shallow fluid in which the spherical radius r is replaced by the earth's mean radius a (Phillips, 1966),

$$\frac{U^2}{a}\tan\phi + fU = -\frac{1}{a}\frac{\partial\Phi}{\partial\phi}. \tag{2.2}$$

U is the zonal flow, ϕ is latitude, Ω is the earth's rotation rate, $f = 2\Omega\sin\phi$ is the Coriolis parometer, and Φ is the geopotential. With the hydrostatic assumption, we use a log pressure coordinate in which $z \equiv \log(p_o/p)$ is the vertical coordinate, with pressure p and a constant reference pressure p_o; temporal and horizontal derivatives are on surfaces of constant pressure. The zonal momentum equation is written in terms of absolute angular momentum $M \equiv a\cos\phi(\Omega a\cos\phi + U)$ (consistent with Phillips' (1966) "traditional approximation" for a shallow fluid):

$$\frac{dM}{dt} \equiv \frac{\partial M}{\partial t} + \frac{V}{a}\frac{\partial M}{\partial \phi} + W\frac{\partial M}{\partial z} = F. \tag{2.3}$$

t is time, $V \equiv a\, d\phi/dt$ is the meridional flow, $W \equiv dz/dt$ is the vertical flow, and F is an arbitrary symmetric torque (which might include a frictional component). The thermodynamic energy equation is

$$\frac{d\theta}{dt} \equiv \frac{\partial \theta}{\partial t} + \frac{V}{a}\frac{\partial \theta}{\partial \phi} + W\frac{\partial M}{\partial z} = Q, \tag{2.4}$$

where Q represents thermal sources. $\theta \equiv Te^{\kappa z}$ is potential temperature, with temperature T; $\kappa \equiv R/c_p$. The continuity equation is

$$0 = \underset{\sim}{\nabla}\cdot(e^{-z}\underset{\sim}{V}) = e^{-z}\frac{\partial(V\cos\phi)}{a\cos\phi\,\partial\phi} + \frac{\partial}{\partial z}(e^{-z}W). \tag{2.5}$$

Finally, the hydrostatic approximation is

$$\frac{\partial \Phi}{\partial z} = RT = Re^{-\kappa z}\theta \tag{2.6}$$

It may be noted that these equations take the Boussinesq form if $e^{\kappa z}$ and e^{-z} are replaced by unity.

The thermal wind relation is obtained by differentiating (2.2) with respect to z and substituting from the hydrostatic relation (2.6). The relationship between angular momentum and potential temperature has a simple form if we substitute the latitudinal coordinate $\mu \equiv \sin\phi$ and a pressure-type height coordinate $\hat{z} \equiv 1-e^{-z} = (p_o-p)/p_o$. These are mass coordinates in that approximately equal amounts of mass are located between constant increments of $\Delta\mu$ or of $\Delta\hat{z}$. $\mu = -1$ at the South Pole, $\mu = +1$ at the North Pole; $\hat{z} = 0$ at the lower boundary ($p = p_o$) and $\hat{z} = 1$ at the top of the atmosphere ($p = 0$). Defining the two geometric functions

$$f_1(\mu) \equiv \frac{\sin\phi}{\cos^4\phi} = \frac{\mu}{(1-\mu^2)^2}$$

and

$$g_1(\hat{z}) \equiv a^2R\, e^{(1-\kappa)z},$$

we find a simple form for the thermal wind relation

$$f_1(\mu)\,\frac{\partial M^2}{\partial \hat{z}} = -g_1(\hat{z})\,\frac{\partial\theta}{\partial\mu} \equiv B, \qquad (2.7)$$

where B is defined here as the baroclinity of the zonal flow.

Following Eliassen's (1952) method for balanced flows, we eliminate the time derivatives of angular momentum in (2.3) and potential temperature in (2.4) by substituting the thermal wind relation (2.7). There results a second order diagnostic equation for the mean meridional streamfunction ψ, which is defined so as to satisfy the continuity equation (2.5):

$$W\, e^{-z} = \frac{\partial\psi}{\partial\mu}, \quad \frac{V}{a}\cos\phi = -\frac{\partial\psi}{\partial\hat{z}}. \qquad (2.8)$$

The streamfunction equation takes the classical form in the $(\mu, \hat{z})$ coordinate system:

$$\frac{\partial}{\partial\mu}(A\frac{\partial\psi}{\partial\mu} + B\frac{\partial\psi}{\partial\hat{z}}) + \frac{\partial}{\partial\hat{z}}(B\frac{\partial\psi}{\partial\mu} + C\frac{\partial\psi}{\partial\hat{z}}) = \frac{\partial}{\partial\mu}(g_1 Q) + \frac{\partial}{\partial\hat{z}}(2f_1 MF). \tag{2.9}$$

$$A \equiv g_1(\hat{z})\,\frac{\partial\theta}{\partial\hat{z}} = (aNHe^{z})^2 \tag{2.10}$$

is a measure of the gravitational restoring force, or static stability, and is proportional to the square of the Brunt-Vaisala frequency, $N^2 \equiv (g/H\theta)\partial\theta/\partial z$. $H = RT/g$ is the local scale height.

$$C \equiv -\,f_1(\mu)\,\frac{\partial M^2}{\partial\mu} = \frac{a^4}{1-\mu^2}(f + \frac{2U}{a}\tan\phi)(f + \zeta) = \frac{a^4\sigma_I^2}{1-\mu^2} \tag{2.11}$$

is a measure of the inertial stability of the vortex. $\eta = f + \zeta$ is the local vertical component of absolute vorticity; it is proportional to the horizontal gradient of absolute angular momentum:

$$f + \zeta = -\,\frac{1}{a^2}\,\frac{\partial M}{\partial\mu}. \tag{2.12}$$

The vertical component (ζ) of relative vorticity on a sphere is defined as $-\partial(U\cos\phi)/a\cos\phi\partial\phi$. The other flow-dependent factor in the inertial stability is proportional to the absolute angular momentum:

$$(f + \frac{2U}{a}\tan\phi) = f(1 + \frac{U}{\Omega a\cos\phi}) = f\,\frac{M}{M_E}, \tag{2.13}$$

where $M_E \equiv \Omega a^2\cos^2\phi$ is the angular momentum of the earth at the surface. The inertial frequency σ_I is just the geometric mean of these two factors, (2.12) and (2.13).

Following Eliassen (1952), the necessary condition for the stability of a baroclinic vortex is that the diagnostic streamfunction

equation (2.9) be elliptic throughout the domain. The ellipticity condition is that the discriminant $D \equiv AC-B^2$ be non-negative everywhere. From (2.7), (2.10) and (2.11), the discriminant can be written

$$D = f_1 g_1 \left(\frac{\partial M^2}{\partial \hat{z}} \frac{\partial \theta}{\partial \mu} - \frac{\partial M^2}{\partial \mu} \frac{\partial \theta}{\partial \hat{z}}\right) = f_1 g_1 \cdot 2M\left(\frac{\partial M}{\partial \hat{z}} \frac{\partial \theta}{\partial \mu} - \frac{\partial M}{\partial \mu} \frac{\partial \theta}{\partial \hat{z}}\right). \tag{2.14}$$

Hoskins (1974) showed that the discriminant on an f-plane is proportional to the potential vorticity q. Thus the condition for instability is that the product of the Coriolis parameter f and the potential vorticity q be negative somewhere in the fluid. In the spherical geometry, a potential vorticity equation for zonally symmetric flow can be obtained after some algebraic manipulation. It is expedited by first noting that for any quantity L,

$$\frac{d}{dt} \frac{\partial L}{\partial s} = \frac{\partial}{\partial s} \frac{dL}{dt} - \frac{\partial \underset{\sim}{V}}{\partial s} \cdot \underset{\sim}{\nabla} L.$$

Here s is either ϕ or z; $\underset{\sim}{V}$ is the velocity vector in the meridional plane, $V\hat{\underset{\sim}{j}} + W\hat{\underset{\sim}{k}}$; $\underset{\sim}{\nabla} \equiv \hat{\underset{\sim}{j}} \frac{\partial}{a\partial\phi} + \hat{\underset{\sim}{k}} \frac{\partial}{\partial z}$; and

$$\frac{d}{dt} \equiv \frac{\partial}{\partial t} + \underset{\sim}{V} \cdot \underset{\sim}{\nabla}.$$

$\hat{\underset{\sim}{i}}$, $\hat{\underset{\sim}{j}}$, $\hat{\underset{\sim}{k}}$ are unit vectors in the longitudinal, latitudinal, and vertical directions.

To obtain the potential vorticity equation, the angular momentum equation (2.3) is operated on by $-\frac{\partial}{a\partial\phi}$ to yield the vorticity equation. Horizontal divergence is eliminated by application of the continuity equation (2.5). The resulting vorticity equation is combined with the horizontally and vertically differentiated thermodynamic equation (2.4)

to obtain

$$\frac{dq}{dt} = \frac{1}{pa\cos\phi}\left(\frac{\partial\theta}{a\partial\phi}\frac{\partial F}{\partial z} - \frac{\partial\theta}{\partial z}\frac{\partial F}{a\partial\phi}\right) + \frac{1}{p}\left[(f+\zeta)\frac{\partial Q}{\partial z} + \frac{\partial U}{\partial z}\frac{\partial Q}{a\partial\phi}\right] \tag{2.15}$$

$$\simeq \frac{1}{pa\cos\phi}\,\hat{\underset{\sim}{i}}\cdot(\underset{\sim}{\nabla}\theta\times\underset{\sim}{\nabla}F) + \frac{1}{p}(2\underset{\sim}{\Omega} + \nabla\times\underset{\sim}{v})\cdot\nabla Q$$

where the potential vorticity q is defined as

$$q \equiv \frac{f+\zeta}{p}\frac{\partial\theta}{\partial z} + \frac{1}{p}\frac{\partial U}{\partial z}\frac{\partial\theta}{a\partial\phi} \simeq (2\underset{\sim}{\Omega}+\underset{\sim}{\nabla}\times\underset{\sim}{V})\cdot\frac{1}{p}\underset{\sim}{\nabla}\theta. \tag{2.16}$$

The approximations in (2.15) and (2.16) are those that follow from substituting a for r in the metric coefficients, following Phillips (1966): specifically the $2\Omega\cos\phi\hat{j}$ component of planetary vorticity $2\underset{\sim}{\Omega}$ does not appear. This neglect does not affect the conclusions drawn in the next section. Note that the meridional momentum equation never enters the derivation; hence potential vorticity conservation is independent of the "balance approximation" (2.2).

Two other expressions for potential vorticity prove useful for physical insight into symmetric circulations. First, as noted by Charney (1973), potential vorticity is proportional to the cross product of the gradient of potential temperature and the gradient of angular momentum. Since the angular momentum gradient is related to the vector vorticity of the absolute tangential flow $U_T \equiv \Omega a\cos\phi + U$ by

$$\hat{\underset{\sim}{i}} \times \frac{-\underset{\sim}{\nabla}M}{a\cos\phi} = \underset{\sim}{\nabla}\times(\hat{\underset{\sim}{i}}U_T) = \hat{j}\frac{\partial U}{\partial z} + \hat{\underset{\sim}{k}}(f+\zeta), \tag{2.17}$$

it immediately follows that

$$q = \frac{\hat{\underset{\sim}{i}}\cdot(\underset{\sim}{\nabla}\theta\times\underset{\sim}{\nabla}M)}{pa\cos\phi}. \tag{2.18}$$

Thus, as discussed by Held and Hou (1980), potential vorticity depends on the relative angle between potential temperature surfaces and angular momentum surfaces. Second, it is easily shown that

$$q = \frac{1}{p_o a^2} \left(\frac{\partial M}{\partial \hat{z}} \frac{\partial \theta}{\partial \mu} - \frac{\partial M}{\partial \mu} \frac{\partial \theta}{\partial \hat{z}}\right). \tag{2.19}$$

Therefore the stability discrimant D can be written

$$D = \frac{p_o a^2}{\Omega} \frac{g_1}{(1-\mu^2)^2} fMq. \tag{2.20}$$

b. Implications for equatorial flow on a sphere

For balanced flow at the equator, Eq. (2.2) implies that the meridional pressure gradient (or geopotential gradient on a pressure surface) must vanish locally. Any north-south pressure gradient will cause an immediate meridional acceleration which will act to eliminate the gradient. This statement and the following argument require that friction be negligible in the meridional momentum equation.

It follows from the hydrostatic approximation (2.6) that the horizontal temperature gradient at the equator also vanishes. The baroclinity B is therefore identically zero at the equator.

We now demonstrate that the zonal flow can have no horizontal shear at the equator for a stable vortex. The inertial stability factor C must vanish at the equator since it is proportional to the Coriolis parameter f (cf. (2.11) and (2.13)). Hence the discriminant D also vanishes locally. For symmetric stability on both sides of the equator, D and therefore C must be positive both north and south of the equator, assuming a statically stable atmosphere with A everywhere positive. Unless the equatorial zonal flow is from the east and greater than 450 m s^{-1}, the angular momentum is positive. Under this assumption, (2.11)

and (2.13) together imply

$$C \propto f(f + \zeta) \geq 0. \tag{2.21}$$

For a stable vortex, then, the absolute vorticity $(f + \zeta)$ must be positive north of the equator ($f > 0$) and negative south of the equator ($f < 0$). In a "smooth" wind field with a continuous vorticity profile, the vorticity ζ must vanish at the equator where f vanishes; otherwise, with any mean flow vorticity at the equator, no matter how small, criterion (2.21) is violated in a region adjacent to the equator. Since the horizontal shear of the mean zonal flow is proportional to the vorticity at the equator, we conclude that there can be no horizontal shear of the mean zonal flow at the equator in a stable axisymmetric vortex.

It necessarily follows that the potential vorticity q must also vanish at the equator. Since the vertical component of vorticity vanishes at the equator, it follows that the absolute vector vorticity, $2\underset{\sim}{\Omega} + \underset{\sim}{\nabla}\times\underset{\sim}{V}$, must lie in the horizontal plane at the equator. Likewise, the gradient of angular momentum is vertical at the equator. Since the gradient of potential temperature is also vertical at the equator, both expressions for potential vorticity, (2.16) in terms of vector vorticity and (2.18) in terms of the angular momentum gradient, imply that potential vorticity vanishes at the equator. For stability ($D > 0$), (2.20) implies q must be positive north of the equator and negative south of the equator.

Finally, the potential vorticity equation (2.15) places a constraint on cross-equatorial flow in a balanced axisymmetric vortex. Since the potential vorticity of a parcel changes sign in balanced

cross-equatorial flow, there must be a local source/sink. Balanced cross-equatorial flow can occur only if there is a north-south gradient in the torque F or in the heat source Q at the equator.

3. Symmetric instability near the equator: beta-plane analysis

In this section we calculate the temporal and spatial characteristics of inertial instability at the equator. By applying the γ-plane assumptions introduced by Boyd (1978a), analytic solutions are obtained in terms of the familiar Hermite functions of equatorial beta-plane theory (Matsuno, 1966; Lindzen, 1967).

Dunkerton (1981) presented an analysis similar to that presented in this section for the inviscid case with linear shear. Here his horizontal structure equation is extended to include the simplest parameterization of dissipation and quadratic as well as linear shear. It is also demonstrated that his results on maximum growth rate and spatial scales of maximum instability are limited by the assumption of a real separation parameter (equivalent depth h). In this section we find symmetric modes of greater instability when complex equivalent depths are considered.

3a. Spatial separation of perturbation equations

Assuming a mean zonal flow $\bar{u}$ with horizontal but no vertical shear, the primitive equations for zonally symmetric perturbations on an equatorial beta-plane are

$$\frac{\partial u'}{\partial t} + v'\frac{d\bar{u}}{dy} - \beta y v' = -\alpha_1 u' \tag{3.1a}$$

$$\frac{\partial v'}{\partial t} + \beta y u' = -\frac{\partial \phi'}{\partial y} - \alpha_1 v' \tag{3.1b}$$

$$\frac{\partial v'}{\partial y} + \frac{1}{p}\frac{\partial p w'}{\partial z} = 0 \tag{3.1c}$$

$$\frac{\partial \phi'}{\partial z} = RT' \tag{3.1d}$$

$$\frac{\partial T'}{\partial t} + \Gamma w' = - \alpha_2 T'. \tag{3.1e}$$

Equations (3.1) are the zonal and meridional momentum equations, continuity equation, hydrostatic approximation, and thermodynamic energy equation in log pressure coordinates. Primed variables represent perturbation quantities. Mechanical and thermal dissipation are represented as Rayleigh friction and Newtonian cooling with spatially and temporally uniform damping time scales, α_1^{-1} and α_2^{-1}, respectively. $y \equiv a\phi$ is latitudinal distance; $\beta \equiv 2\Omega/a = (df/dy)_{Equator}$; Γ is the static stability in log p coordinates, assumed to be a function of height only. The small latitudinal gradients of geopotential and static stability that accompany a geostrophic mean zonal flow are dynamically unimportant and therefore are neglected.

Because the mean zonal flow depends only on latitude, the perturbation equations are separable in their temporal, horizontal, and vertical structure. Assuming that each perturbation field can be described as an exponential function of time $e^{-i\hat{\sigma}t}$, where $\hat{\sigma}$ is the complex frequency, multiplied by a function of height and a function of latitude, the problem separates into a vertical structure equation and a set of horizontal structure equations. The vertical structure equation is

$$\frac{1}{p}\frac{d}{dz}\frac{p}{R\Gamma}\frac{\sigma_2}{\sigma_1}\frac{dG}{dz} + \frac{1}{gh}G = 0, \tag{3.2}$$

where G is the vertical structure component of u', v', and Φ'. $\sigma_1 = \hat{\sigma}+i\alpha_1$ and $\sigma_2 = \hat{\sigma}+i\alpha_2$ represent the complex frequencies with dissipation. The separation constant is the equivalent depth h. The

horizontal structure equations are

$$- i\sigma_1 u - (\beta y - \frac{d\bar{u}}{dy})v = 0 \tag{3.3a}$$

$$- i\sigma_1 v + \beta y u = - \frac{d\Phi}{dy} \tag{3.3b}$$

$$- i\sigma_1 \Phi + gh \frac{dv}{dy} = 0. \tag{3.3c}$$

u, v, Φ are the horizontal structure components of u', v', Φ', respectively. Eqs. (3.3) are the shallow water equations for a fluid of mean depth (real) h <u>if</u> mechanical dissipation is negligible ($\alpha_1 = 0$, $\sigma_1 = \hat{\sigma}$) and the mean zonal flow $\bar{u}$ vanishes. In the more general shallow water equations, a non-zero mean zonal flow must be balanced geostrophically by a height gradient ($d\bar{h}/dy$) which causes an additional term $vg(d\bar{h}/dy)$ to contribute to the mass divergence of Eq. (3.3c).

3b. <u>Solution of the horizontal structure equations</u>

The horizontal structure equations are easily combined into a single second-order equation for v:

$$gh \frac{d^2v}{dy^2} + [\sigma_1^2 - \beta y(\beta y - \frac{d\bar{u}}{dy})]v = 0. \tag{3.4}$$

The second factor in brackets represents the square of the local inertial frequency on a beta-plane:

$$\sigma_I^2 = \beta y(\beta y - \frac{d\bar{u}}{dy}) = f(f + \bar{\zeta}). \tag{3.5}$$

We find that σ must be real or pure imaginary if the equivalent depth is real and if the meridional wind satisfies homogeneous boundary conditions at the northern (y_N) and southern (y_S) boundaries. Multiplying (3.4) by the complex conjugate of v, v*; subtracting the complex conju-

gate of (3.4) times v; and then integrating over the domain, we find

$$gh[v^* \frac{dv}{dy} - v \frac{dv^*}{dy}]_{y_S}^{y_N} + (\sigma_1^2 - \sigma_1^{*2}) \int_{y_S}^{y_N} v^* v dy = 0. \tag{3.6}$$

Since the first term vanishes, for non-trivial solutions we have

$$\sigma_1^2 - \sigma_1^{*2} = 0. \tag{3.7}$$

Thus for real equivalent depths, σ_1 must be real or pure imaginary. This result does not hold for the more general case of complex equivalent depths, as is shown below by explicit calculation.

Following Boyd (1978a), the zonal wind structure in the vicinity of the equator is represented as a quadratic function of y:

$$\bar{u} = U_o + \gamma y + \tfrac{1}{2}\delta y^2 \tag{3.8}$$

The second-order v equation (3.4) can then be solved exactly on the unbounded beta-plane by transforming the horizontal coordinate. Unlike the cases treated by Boyd involving asymmetric perturbations (e.g., Kelvin and mixed Rossby-gravity waves), no approximation of the index of refraction [bracketed quantity in (3.4)] is necessary. Figure 3 displays typical flow geometries for (a) a westerly jet, with negative curvature δ; (b) linear shear flow with no curvature; and (c) an easterly jet, with positive curvature. Whenever there is horizontal shear at the equator ($\gamma \neq 0$), there is a region adjacent to the equator where the absolute vorticity $\bar{\eta}$ of the mean zonal flow has a sign opposite to that of the local planetary vorticity f; in Figure 3, this region is indicated by hatching. According to Section 2b, this should be the region of inertial instability. For a westerly jet, this region is on the jet side of the equator (assuming $\beta - \delta > 0$). For an easterly jet,

this region is on the opposite side of the equator. It is bounded by the equator (y = 0) and the latitude where the absolute vorticity $\bar{\eta}$ vanishes. Defining this latitude to be a distance $2y_o$ from the equator, we find that with

$$\bar{\eta} = f + \bar{\zeta} = f - \frac{d\bar{u}}{dy} = (\beta - \delta)y - \gamma, \tag{3.9}$$

$\bar{\eta} = 0$ at

$$y = 2y_o \equiv \frac{\gamma}{\beta-\delta}. \tag{3.10}$$

The center of this region is at $y = y_o$.

Let us define ξ as a scaled latitudinal coordinate centered on the equator:

$$\xi = y/\ell \tag{3.11}$$

where $\beta_a^2\ell^4 = gh$ and $\beta_a^2 \equiv \beta(\beta - \delta)$. (3.12)

β_a is an adjusted beta when quadratic shear flow is included. Again it is assumed that $\beta - \delta > 0$ in order that trapped equatorial solutions exist. This implies that barotropic instability is not possible according to the conventional necessary condition ($\beta-\delta=0$ somewhere) for this type of asymmetric instability. The length scale ℓ depends on the equivalent depth h and the flow curvature δ. For linear shear flow (δ = 0), ℓ is the standard horizontal length scale on the equatorial beta-plane (Lindzen, 1967). If we use this dynamically scaled variable, but shifted so that it is centered at latitude y_o [which, following Boyd (1978a), may be considered the "dynamic equator"], we obtain the canonical form of the v-equation. Specifically, defining the coordinate $\nu = \xi - \xi_o$, where $\xi_o \equiv y_o/\ell$, the v-equation becomes

$$\frac{d^2v}{d\nu^2} + [(\frac{\sigma_1^2}{\beta_a^2 \ell^2} + \xi_o^2) - \nu^2]v = 0. \tag{3.13}$$

The solutions which remain bounded as $y \to \pm\infty$ on the infinite beta-plane have eigenvalues

$$\frac{\sigma_1^2}{\beta_a^2 \ell^2} + \xi_o^2 = 2n + 1, \quad n = 0, 1, 2, \ldots \tag{3.14}$$

with eigenfunctions

$$v_n = C_n H_n(\nu) e^{-\frac{1}{2}\nu^2}. \tag{3.15}$$

$H_n(\nu)$ is the $n^{\underline{th}}$ order Hermite polynomial; C_n is an arbitrary constant which we will use later to normalize the eigenfunctions. For the zonally symmetric problem, there is no analog to the asymmetric (n = -1) Kelvin mode with v = 0. The dispersion relation (3.14) can be rewritten in the form

$$\sigma_1^2 = \beta_a \sqrt{gh}\,(2n + 1) - (\frac{\gamma}{2})^2 (\frac{\beta}{\beta_a})^2. \tag{3.16}$$

In the absence of shear ($\gamma = \delta = 0$), the frequency σ is real and the flow is inertially stable. However, with non-zero equatorial shear ($\gamma \neq 0$), no matter how small, σ_1^2 becomes negative, indicating instability, for sufficiently small (real) equivalent depth and horizontal mode number n. Hence the inertial instability is manifested most readily in the smallest vertical scales, which according to Eq. (3.2) correspond to the smallest equivalent depths, and in the gravest (n = 0) latitudinal mode. For unstable modes, σ_1 is pure imaginary ($\sigma_1 = i\sigma_i$) and the maximum growth rate is proportional to the equatorial shear:

$$\sigma_{i,max} = \left|\frac{\gamma}{2}\right| \frac{\beta}{\beta_a} \tag{3.17}$$

When the curvature δ is much smaller than β, the maximum growth rate is approximately one-half the magnitude of the relative vorticity of the mean flow at the equator. For example, with a latitudinal shear of 1 ms^{-1} per 100 km, the e-folding time for the instability is 2.3 days.

Up to this point, the results derived here amount to a generalization of the rather cryptic analysis of Dunkerton (1981) for an inviscid fluid with linear shear. If mechanical dissipation is present in the form of the linear damping coefficient α_1, the growth rate $\hat{\sigma}_i$ is reduced from that calculated above by an amount equal to the dissipation rate: i.e.,

$$\hat{\sigma}_i = \sigma_i - \alpha_1.$$

Hence this form of the instability ($\hat{\sigma}_i > 0$) can only occur if $\sigma_{i,max}$ of (3.17), which depends only on the mean flow parameters, is greater than the dissipation rate α_1. The thermal dissipation does not affect the stability criterion.

Dunkerton realized that this form of dissipation does not affect the scale of maximum instability. Vertical diffusion which is scale-dependent stabilizes the smallest scales and therefore produces an intermediate scale of maximum instability. This dissatisfaction with smallest-scale instability appears to be the sole rationale for choosing a second-order representation of the mechanical diffusion.

In the next section it is shown that modes of greater instability than Dunkerton's do exist at finite scales.

3c. Symmetric instability with complex equivalent depth

Dunkerton limited his search for instabilities to real values of the separation parameter in (3.2) and (3.4), the equivalent depth h. However, it is notable that previous studies of hydrodynamic/thermodynamic instabilities have found applicable instabilities with complex equivalent depths. The studies of Hayashi (1970), Lindzen (1974), Stevens and Lindzen (1978), and others have utilized this concept in investigating the cooperative interaction between tropical waves and cumulus convection. It turns out that consideration of complex equivalent depths yields completely different results from those of Dunkerton.

For notational convenience, define $c^2 \equiv gh$ as an alternative form for the separation constant. Let us explicitly consider the behavior of the complex frequency as a function of c. In this section, unlike the previous one with only real values of c, we will need to consider the vertical structure of the solutions: the thermal dissipation α_2 therefore enters the analysis. For illustrative simplicity, we focus on the case with equal (constant) values of mechanical and thermal dissipation, $\alpha_1 = \alpha_2 = \alpha$. The results of this section can be easily extrapolated to the more general case. It will be apparent that the effect of dissipation is exactly as discussed at the end of Section 3b -- namely, a reduction of the instability rate $\hat{\sigma}_i$ by an amount α. With $\alpha_1 = \alpha_2 = \alpha$, the complex frequencies also become equivalent, $\sigma_1 = \sigma_2 = \sigma$.

Figure 4 presents the real and imaginary parts of the complex frequency $\sigma = \sigma_r + i\sigma_i$ for complex $c = c_r + ic_i$. $c_r = 1\ ms^{-1}$ is specified and c_i is allowed to vary. Since we are concerned with instability, only the root of (3.16) with positive growth rate σ_i is investigated. $\gamma = 10^{-5}s^{-1}$, $\delta = 0$, and $n = 0$ are assumed. It is clear from Figure 4

that the instability with real equivalent depth ($c_i = 0$) actually has a minimum in growth rate σ_i when compared with complex equivalent depths. Thus the modes found by Dunkerton are least (not most) unstable if this more general set of modes is available. The character of the modes differs substantially in that they propagate in the meridional direction with $\sigma_r \cong \sigma_i$ for $c_i \gtrsim c_r$. As c_i increases, growth rate σ_i increases without bound. Also plotted is the non-dimensional vertical wavenumber $\lambda = \lambda_r + i\lambda_i$ in log p coordinates which represents a solution of (3.2) if the stability Γ is assumed constant. $R = 287$ J $kg^{-1}K^{-1}$ and a representative value of $\Gamma = 40$ K have been assumed in calculating the vertical wavenumber. For a given value of λ plotted in Fig. 4, $-\lambda$ is also an appropriate wavenumber solution to (3.2). The formal solutions (G) of (3.2) have the form $\exp[(i\lambda+\frac{1}{2})z]$, where

$$\lambda^2 = \frac{R\Gamma}{gh} - \frac{1}{4} \quad . \quad . \qquad (3.18)$$

Wavenumber is inversely proportional to the vertical scale of the eigensolution: thus $\lambda = 1$ indicates one scale height (H) as the vertical scale, while $\lambda = 10$ indicates that the vertical scale is H/10. From Fig. 4, we see that maximum instability occurs at maximum vertical scale. In fact, the instability approaches a barotropic structure (G constant with height) as c_i and σ_i increase.

To represent a valid eigensolution, the eigenfunction must be bounded on the (assumed) infinite equatorial beta plane. With complex eigenvalues, the horizontal scale ℓ in (3.11) and (3.12) is complex. Thus we require that $\exp[-\frac{1}{2}(y-y_o)^2/\ell^2]$ be bounded as $y \to \pm\infty$; i.e., $\mathrm{Re}(\ell^{-2})>0$. Since $\ell^2 = c/\beta_a$ from (3.12), and $\beta_a > 0$ has been assumed, it

follows that $c_r > 0$ for boundedness. Additionally, in the semi-infinite atmosphere, energy density associated with the solution must be bounded as $z \to \infty$. This constraint implies $\lambda_i \geq 0$. These conditions are met in the solutions considered in this paper.

Since $\ell^2 = c/\beta_a$, the most unstable solutions occur at maximum horizontal as well as vertical scale -- a result exactly opposite to Dunkerton's. In this limit, our model assumptions break down. It is unrealistic to allow solutions which depend on $f = \beta y$ becoming large or on the infinite winds of pure linear or quadratic shear flow on the infinite beta plane. To obtain the actual allowed growth rates, it is necessary to solve the horizontal/vertical eigenvalue problem numerically: such an approach is currently in progress. However, an estimate of the maximum growth rate can be obtained by assuming that the eigensolution is limited in meridional scale to a pre-assigned horizontal length scale L. This scale might reasonably be assumed as the meridional distance over which the linear/quadratic representation (3.8) of the mean zonal flow is a valid approximation to the observed flow. If the eigenfunction is limited to the domain $|y-y_o| \lesssim L$, then the eigensolution should not depend crucially on the wind beyond this domain. In addition, the solutions should not extend beyond one earth's radius ($L \lesssim a$) for βy to be a valid approximation to f and for the neglect of curvature to be a reasonable approximation.

Because the independent variable in (3.13) and (3.15) takes on complex values, we cannot refer to the usual diagrams of real Hermite functions to evaluate the scale of the various solutions. Unlike the neutral analog, with complex ℓ the shape of the complex eigenfunctions v_n vary, depending on the phase of ℓ. Nevertheless, we can obtain some

guidance from the neutral eigensolutions to (3.13). First, we assume the integral values of n in (3.14) are applicable for the boundedness of the eigenfunctions, and therefore the Hermite functions (3.15) with complex argument are still the eigenfunctions. Second, the turning points at which the square of the meridional index of refraction vanishes for the neutral case are located at $\nu^2 = 2n+1$; the solutions decay exponentially beyond these latitudes. We require that the unstable solutions be primarily confined to the region $\mathrm{Re}(\nu^2) \lesssim 2n+1$; this constraint is sufficient to determine a maximum magnitude of the separation constant c for a specified horizontal scale L. It will be shown a posteriori that this is not a bad estimate for the maximum scale of the eigenfunctions. It is important to realize that L is not the usual scale of variation in the y-direction; rather, it is the domain over which the eigenfunction is non-negligible.

Requiring $\mathrm{Re}(\nu^2) \leq 2n+1$ at the points $\left|y-y_o\right| = L$, we find that the complex separation constant $c = c_r+ic_i$ is limited by the constraint

$$c_r^2 + c_i^2 \leq \frac{c_r c_s}{2n+1} , \tag{3.19}$$

where $c_s \equiv \beta_a L^2$. This implies that $c_r \leq c_s/(2n+1)$ and that $c_i \leq c_r^{\frac{1}{2}}[c_s/(2n+1)-c_r]^{\frac{1}{2}} \leq \frac{1}{2}\, c_s/(2n+1)$. Table 1 shows the maximum c_r for several values of n and L, and maximum c_i for several values of n, L, and c_r. Linear shear ($\delta = 0$, $\beta_a = \beta$) is assumed.

Since the largest allowable c_i in Table 1 occur with the gravest (n = 0) horizontal mode, we consider the growth rates associated with this mode. Figure 5 displays the growth rates for the n = 0 mode and c_r ranging from 0.01 to 100 m s^{-1}. As in Fig. 4, $\delta = 0$, $\beta = \beta_a$, and $\gamma = 10^{-5}$ s^{-1} are assumed. Growth rate increases monotonically with c_i for a

given c_r (as in Fig. 4); it also increases monotonically as c_r decreases for a given c_i. The maximum allowable growth rate is extremely sensitive to the domain scale L. If L = 3000 km, maximum growth rate is $2.2 \cdot 10^{-5} s^{-1}$, over four times greater than the maximum of $0.5 \cdot 10^{-5} s^{-1}$ found in the previous section with real c. With L = 1000 km, $\sigma_{i,max} \simeq 0.8 \cdot 10^{-5} s^{-1}$. With L = 300 km, $\sigma_{i,max} \simeq 0.5 \cdot 10^{-5} s^{-1}$, the same as with real c. We notice that a transition occurs between L = 300 km and L = 1000 km which allows higher growth rates and markedly different structures with larger domain size L in comparison with the purely real separation constants. The most unstable modes then have substantially larger scales than the inviscid modes found by Dunkerton (1981), which are most unstable in the limit of smallest vertical scale.

Furthermore, these modes are much less affected by dissipation. Focusing on the case with L = 1000 km, the Rayleigh friction must have a time scale faster than the e-folding time of 1.5 days to eliminate the instability. If a second-order diffusion parameterization is used, the time scale $H^2/|\lambda|^2 \nu$ must be faster than σ_i^{-1} to eliminate instability: with $H \simeq 7$ km and $|\lambda| \simeq 5$, stability would require an eddy viscosity $\nu \gtrsim 15\ m^2 s^{-1}$.

For a given c_r, higher order modes can now be more unstable than the gravest n = 0 mode. Fig. 6 shows the growth rate as a function of c_i for $c_r = 1\ ms^{-1}$ and modes n = 0, 2, 4. For L = 1000 km, the n = 2 mode is most unstable; for L = 3000 km, n = 4 is the most unstable of the three modes, and higher modes are even more unstable.

The asymptote as $c_i \to 0$ for n = 0 is very different from those for n = 2, 4. The character of the asymptote can be obtained from (3.16). It depends on the parameter

$$E_n \equiv \frac{2n+1}{2} \left(\frac{2}{\gamma} \frac{\beta_a}{\beta}\right)^2 \beta_a c_r \tag{3.20}$$

If $2E_n << 1$, in the limit $c_i \to 0$,

$$\sigma_r \cong \frac{2n+1}{2} \left(\frac{2}{\gamma} \frac{\beta_a}{\beta}\right) \beta_a c_i \tag{3.21a}$$

$$\sigma_i \cong \left(\frac{\gamma}{2} \frac{\beta}{\beta_a}\right) \left[1 - E_n - \tfrac{1}{2} E_n^2 \left(1 - \frac{c_i^2}{c_r^2}\right)\right] \tag{3.21b}$$

If $2E_n >> 1$, in the limit $c_i \to 0$,

$$\sigma_r \cong \left(\frac{\gamma}{2} \frac{\beta}{\beta_a}\right) \sqrt{2E_n - 1} \tag{3.22a}$$

$$\sigma_i \cong \left(\frac{\gamma}{2} \frac{\beta}{\beta_a}\right) \frac{E_n}{\sqrt{2E_n - 1}} \frac{c_i}{c_r} \tag{3.22b}$$

For the parameters of Fig. 6, $E_o = 0.458$, $E_2 = 2.289$, $E_4 = 4.121$.

In the limit $c_i \to \infty$ for fixed c_r, σ_r and σ_i approach the same limit which is independent of the shear γ:

$$\sigma_r \cong \sigma_i \cong \sqrt{\beta_a c_i \frac{2n+1}{2}} \,. \tag{3.23}$$

As already discussed, this limit is inappropriate for equatorial modes.

From both Figures 5 and 6, we find that greatest instability tends to occur when c_r and c_i are approximately equal. Fig. 7a displays both σ_r and σ_i for $n = 0$ and the cases where (A) $c_r = c_i = c_o$ (solid) and, for comparison, (B) $c = c_r = c_o$ (dashed). In case (B) where c is real, $\sigma_r = 0$ for $c_o < \gamma^2/4\beta$, and $\sigma_i = 0$ for $c_o > \gamma^2/4\beta$. At small values of $c_o << \gamma^2/4\beta$, the instabilities with real or complex separation constant have similar temporal behavior: in both cases $\sigma_i \to \frac{1}{2}\gamma$ as $c_o \to 0$; in (A) $\sigma_r << \sigma_i$ and (B) $\sigma_r = 0$. However, the vertical structure differs substantially, as seen in Fig. 7b. With complex c, the modes are strongly

trapped in the vertical since λ_i ($\cong -\lambda_r$) is large. For real c, the eigenmode is a vertically propagating mode [$\lambda_i = 0$ for $c_o < (4R\Gamma)^{\frac{1}{2}}$].

When $c_o >> \gamma^2/4\beta$, we see in Fig. 7a that $\sigma_r > \sigma_i$. For a fixed ratio c_i/c_r, the asymptote (3.23) is inappropriate. Writing $c = c_o\sqrt{2}\, e^{i\theta}$ and $c_2 = [\beta_a(2n+1)c_o\sqrt{2}]^{\frac{1}{2}}$, in the limit $c_o \to \infty$,

$$\sigma_r \cong c_2 \left[1-\frac{1}{2c_2^2}\left(\frac{\gamma}{2}\frac{\beta}{\beta_a}\right)^2\right] \cos\frac{\theta}{2} \cong c_2 \cos\frac{\theta}{2} \tag{3.24a}$$

$$\sigma_i \cong c_2 \left[1+\frac{1}{2c_2^2}\left(\frac{\gamma}{2}\frac{\beta}{\beta_a}\right)^2\right] \sin\frac{\theta}{2} \cong c_2 \sin\frac{\theta}{2} \tag{3.24b}$$

$$\frac{\sigma_i}{\sigma_r} \cong \tan\frac{\theta}{2} \tag{3.24c}$$

In Fig. 7a, $\theta = 45°$ and $c_2 = (.569\cdot 10^{-5} m^{-\frac{1}{2}} s^{-\frac{1}{2}})\, c_o^{\frac{1}{2}}$. Since $\tan(22.5°) = 0.414$, σ_r is about 2.4 times larger than σ_i. Indeed, for $c_o > \gamma^2/4\beta$, $\sigma_r > \sigma_i$. This implies that the instability is propagating in the meridional plane as it intensifies. To determine the direction of propagation, we must consider the corresponding eigenfunctions.

Fig. 8 displays the first three symmetric (in v) meridional eigenfunctions (n = 0, 2, 4) for case A ($c_r = c_i = c_o$) and the more standard case B with real c ($c = c_r = c_o$). The eigenfunctions have been normalized to unit area. The phase of all three eigenfunctions of case A increases monotonically with distance from the dynamic equator, both to the north and south. Since $\sigma_r > 0$, we conclude that these unstable modes propagate poleward. We also observe that all three eigenfunctions of case A are essentially contained within the latitudes where $\mathrm{Re}(\nu^2) = 2n+1$, as was assumed earlier. They are <u>not</u> contained within the latitudes where $|\nu|^2 = 2n+1$, an alternative assumption which is not justifiable <u>a posteriori</u>.

3d. Spatial structure and dynamic balances of unstable modes ($\sigma_i > 0$)

In order to further understand the mechanism driving the instability, we consider here the dynamic structure of the unstable eigenfunctions. For simplicity, the instability with real separation constant is studied. The eigenfunctions with c "almost real" ($\left|c_i/c_r\right| \ll 1$) are very similar.

After introducing the symbols for quadratic shear flow in (3.8) the horizontal structure equations (3.3) can be written in terms of the dimensionless coordinate ν:

$$\left(\frac{\sigma_i}{\beta_a \ell}\right) u - \frac{\beta_a}{\beta} (\nu - \xi_o) v = 0 \tag{3.25a}$$

$$\left(\frac{\sigma_i}{\beta_a \ell}\right) v + \frac{\beta}{\beta_a} (\nu + \xi_o) u = - \frac{d}{d\nu}\left(\frac{\Phi}{\sqrt{gh}}\right) \tag{3.25b}$$

$$\left(\frac{\sigma_i}{\beta_a \ell}\right) \frac{\Phi}{\sqrt{gh}} + \frac{dv}{d\nu} = 0 \tag{3.25c}$$

Here $\sigma_i \equiv \mathrm{Imag}(\sigma_1)$ and $\sigma_r = 0$ according to (3.7).

Figure 9 displays the horizontal structure of u, v, and $\Phi/\sqrt{gh}$ in the case of linear shear flow ($\delta = 0$, $\beta_a = \beta$). The n = 0 mode is shown for the cases $\xi_o = 2$ (solid line) and $\xi_o = 10$ (dashed line). The higher value of ξ_o represents a mode of much smaller equivalent depth, since for two modes 1 and 2,

$$\frac{\xi_{o,1}}{\xi_{o,2}} = \frac{\ell_2}{\ell 1} = \left(\frac{h_2}{h_1}\right)^{\frac{1}{4}} \quad . \tag{3.26}$$

For unstable modes ($\sigma_i > 0$), the u-momentum equation (3.25a) requires that u and v have opposite signs, since $\nu - \xi_o < 0$ throughout the region of significant amplitude. In the region from $\nu = -\xi_o$ to $\nu = \xi_o$,

advection of mean zonal momentum dominates the Coriolis force. If for definiteness we consider a mean zonal flow that is increasingly westerly (positive) toward the north, $\gamma > 0$ and the unstable region is located in the Northern Hemisphere. Northward advection ($v > 0$) of the low angular momentum air from the equator tends to decelerate the zonal flow ($\sigma_i u$, $u < 0$). At the same time, this easterly perturbation is turned to the north by the Coriolis force in the v-momentum equation (3.25b), reinforcing the original northward flow and thus providing the instability. Southward flow at another vertical level is similarly enhanced by the positive feedback. The pressure gradient force plays only a minor role in the dynamic instability: geopotential changes and the associated temperature and vertical velocity perturbations are necessary to balance the horizontal convergence of air in the mass budget (3.25c); but as shown in Figure 10 with $\xi_o = 2$, the pressure gradient force is much smaller than the Coriolis force in the v-momentum equation. As the horizontal and vertical scales decrease (i.e., smaller equivalent depths), the dashed lines for u and $\Phi/\sqrt{gh}$ in Figure 9 indicate that the pressure gradient force becomes negligible. For $\xi_o = 10$, the ratio of maximum amplitudes for the pressure gradient force: Coriolis force: acceleration (at $\nu = 0$) is -1: 100: 99.

The instability gains energy from the kinetic energy by means of the barotropic conversion term, $- \int u'v'(d\bar{u}/dy)dy$. From Figure 9, this term is clearly positive. Although the conversion is barotropic in type, it occurs in the highly baroclinic internal modes of small vertical scale. Figure 11, which is similar to Dunkerton's (1981) Fig. 1, shows schematically the structure of an unstable perturbation in the y-z plane. u' and v' are opposite in sign, causing air with high angular

momentum to be transported to the equator at one level, while low-momentum equatorial air is moved poleward at another level. The result is to mix the absolute angular momentum so that the fluid can arrive at a stable configuration with maximum absolute angular momentum located at the equator. The centers of low and high pressure tend to retard the meridional flow, but the Coriolis force overcomes the adverse pressure gradient force, as shown in Figure 10.

4. Discussion

In Section 3, we calculated maximum growth rates for symmetric instability at the equator on the order of the vorticity of the equatorial mean zonal flow. We now consider the applicability of this result to the actual atmosphere and ocean and to model studies.

The equatorial beta-plane analysis assumed that the mean zonal flow depended only on latitude and not on height. This assumption was made in order to obtain an analytic solution separable in its horizontal and vertical structure. However, the instability will also occur in a vertically sheared zonal flow, as shown in the analysis of balanced flow on a sphere in Section 2. Boyd (1978a) has shown that the horizontal structure of the mean zonal flow largely determines perturbation characteristics if the vertical shear is weak; i.e., if the vertical scale of variation of the mean flow is much greater than the vertical scale of the perturbation. Dunkerton (1981) pointed out that this instability mechanism is applicable in regions of weak vertical shear. For stronger shear, as in a jet, the problem is non-separable in its y and z dependence and therefore requires numerical procedures and a significant amount of computation to determine the structure of the instabilities. At the center of an atmospheric jet or oceanic undercurrent, the smallest-scale instabilities with growth rate $\sigma_i \cong \left|\frac{1}{2}\gamma\beta/\beta_a\right|$ should be physically realizable so long as dissipation is insufficient to stabilize the relevant modes.

The analysis of Section 3 also assumed a quadratic structure for the horizontally varying zonal flow. It might be argued that this assumption is unreasonable because the mean flow must become unrealistically large at sufficient meridional distance from the equator.

However, the character of the instability will be primarily determined by its environment in the region of significant perturbation amplitude. For real c, this region is bounded by the equator and the latitude ($2y_o$) where the absolute vorticity vanishes. For complex c, the relevant domain is $y_o-L<y<y_o+L$. Outside this region, the particular flow structure is unimportant since the perturbation amplitude is exponentially small at a sufficient distance from the dynamic equator, as assumed in Section 3.

Many recent model studies of both atmospheric and oceanic circulations have investigated the effect of a horizontally varying mean flow on both neutral waves and unstable asymmetric perturbations. Some of these (e.g., Philander, 1979; Dunkerton, 1982a) investigated mean zonal flows with north-south symmetry about the equator ($\gamma = 0$) which are stable according to this analysis.

Others, however, studied cases with non-zero equatorial shear. Boyd (1978b) considered the effect of horizontal shear flow ($\gamma = 10^{-5}s^{-1}$; $|2/\gamma| = 2.3$ days) on atmospheric Kelvin and mixed Rossby-gravity waves. Philander (1978) found asymmetric barotropic instabilities with e-folding times on the order of two weeks with a realistic zonal flow profile in which $|\gamma| \sim 10^{-6}s^{-1}$ ($|2/\gamma| \sim 23$ days). McPhaden and Knox (1979) used a two-layer oceanic model with the shallow-water equations to look at neutral modes (both symmetric and asymmetric) in the presence of non-zero equatorial shear ($|\gamma| \sim 10^{-5}s^{-1}$). The results of Section 3 imply that none of these assumed basic state flows are appropriate because they cannot be stable solutions of the symmetric governing equations. Dissipation acts to stabilize the zonal flow; however, it does not play the dominant role found by Dunkerton (1981)

when complex eigenvalues are considered, since the smallest scales are no longer preferred. Several of these instability and wave studies have assumed inviscid conditions in deriving conclusions. To the extent that dissipation may be neglected or plays a secondary role, the zonally symmetric instability must be reckoned with in wave and instability studies in the vicinity of the equator.

Holton (1979) made a similar study of the role of latitudinal shear on stratospheric waves with $\gamma \sim 10^{-5} s^{-1}$ ($|2/\gamma| \sim 2.3$ days), but integrated the governing equations for both the mean flow and the perturbations forward in time, rather than looking for normal modes. Despite the relatively fast inferred growth rate, his calculation remained stable for 60 days. This lack of instability can be explained as a result of two factors: first, a dissipation time scale of a few days opposed the symmetric instability; second, the horizontal grid resolution of a few degrees in latitude disallowed the smallest scale modes. Section 3 implies that a horizontally continuous model with somewhat longer and more realistic dissipation time scales would have manifested the symmetric instability.

The effect of the instability studied in this paper is to symmetrize mean zonal flows about the equator, eliminating any horizontal shear in the flow right at the equator. It is proposed that this mechanism causes the approximate north-south symmetry observed in the atmosphere (Figure 1) despite the influences of topography. Holton (1979) showed that equatorial Kelvin and mixed Rossby-gravity waves also act to reduce the horizontal shear at the equator.

The instability mechanism similarly tends to center tropical oceanic currents (Fig. 2) on the equator. For example, we may describe a zonal jet functionally in the form

$$\bar{u} = U_1 \left[1 - \left(\frac{y-y_1}{y_c}\right)^2\right]. \tag{4.1}$$

This quadratic jet has maximum amplitude U_1 at $y = y_1$ and falls to zero speed at $y = y_1 \pm y_c$. In terms of the parameters of Section 3, $U_0 = U_1(1-y_1^2/y_c^2)$, $\gamma = 2U_1 y_1/y_c^2$, and $\delta = -2U_1/y_c^2$. The maximum growth rate $\sigma_{i,max}$ of (3.17) is proportional to the distance $|y_1|$ of the jet core from the equator:

$$\sigma_{i,max} = \left|\frac{U_1 y_1}{y_c^2}\right| \left(1 + \frac{2U_1}{\beta y_c^2}\right)^{-\frac{1}{2}} \tag{4.2}$$

The equatorial undercurrent might be modeled with the parameters $U_1 = 50$ cm s^{-1} and halfwidth $y_c = 100$ km. If the center of the current were located at $y_1 = \pm 100$ km, the instability would have a minimum e-folding time scale of about 5 days. As mentioned above, this instability mechanism can operate only if the dissipation time scale is longer than the e-folding time scale of instability.

One further application of the symmetric instability is the phenomenon of poleward-propagating, zonally symmetric oscillations in the tropics, recently analyzed by Anderson and Rosen (1982) and Krishnamurti (1982). Anderson and Rosen (1982) have suggested that these quasi-periodic motions are the zonally averaged part of the 40-50 day circulations described by Madden and Julian (1971, 1972). The characteristics of the theoretically-predicted symmetric instability are so similar to the observed systems that this instability mechanism may be considered

a candidate for the dynamical forcing of the oscillations. According to Fig. 9 of Anderson and Rosen (1982), these tropospheric oscillations in the zonal flow display (1) approximate symmetry about a near-equatorial latitude, with one maximum on each side of the equator between 30 S and 30 N; (2) baroclinic structure which is confined to the tropics (with barotropic structure in middle latitudes); and (3) phase propagation which is poleward and downward. Using $\gamma = 10^{-5}s^{-1}$, $\delta = 0$, $c = (1+i)\cdot 10$ ms^{-1}, and $n = 1$, the theoretical instability (1) is only approximately symmetric in amplitude with respect to a near-equatorial latitude, having two maxima of unequal size; (2) is equatorially trapped, with negligible amplitude poleward of 30 N and 30 S; (3) is baroclinic in nature, with $-\lambda_r \cong \lambda_i \cong 5$; and (4) propates poleward and downward. The time scale of this mode is much faster than the observed 40-50 day period if dissipation is ignored; however, neglected aspects, such as non-linearity, vertically sheared basic flow, topography, zonal asymmetry, and higher-order dissipation, could have a large effect on the time scale.

5. Summary

Observations of longitudinally-averaged zonal flows in the atmosphere and ocean tend to display north-south symmetry about the equator, with a characteristic wind maximum or minimum and therefore little horizontal wind shear locally near the equator. It has been shown that this configuration is required for balanced flow on a sphere to be inertially stable. Any horizontal wind shear at the equator will cause a symmetric instability to develop, effectively eliminating the horizontal shear. It follows that the potential vorticity must vanish at the equator. Balanced cross-equatorial flow can occur only if there is a north-south gradient in the torque or the diabatic heating at the equator. These conclusions are obtained under the assumption of a balanced zonal flow; i.e., acceleration and dissipation have been explicitly neglected in the meridional momentum equation.

The characteristics of the equatorial symmetric instability that develops if the mean flow is horizontally sheared at the equator are investigated. The analysis with Rayleigh friction and Newtonian cooling follows and extends the brief treatment of inviscid instability on the equatorial beta-plane by Dunkerton (1981). Quadratic as well as linear shear is considered.

If only real values of the separation constant (equivalent depth h) are considered, so that vertical wavenumber is real, Dunkerton's results are reproduced. The instability is confined to the region in which the vertical component of absolute vorticity is of opposite sign to the local Coriolis parameter; i.e., where the square of the inertial frequency is negative. The mode of greatest instability is a meridional overturning with a single cell in the horizontal dimension which tends

to mix angular momentum, thereby eliminating the horizontal gradient of angular momentum at the equator. With this particularly simple parameterization of mechanical and thermal dissipation, the mixing occurs most readily at the smallest vertical scales and the gravest (n = 0) meridional mode. When the flow curvature is much less than β, the maximum growth rate for symmetric instability is approximately one-half the magnitude of the relative vorticity of the mean flow at the equator minus the mechanical dissipation rate. Hence the horizontal shear at the equator must exceed twice the Rayleigh friction coefficient for instability. Thermal dissipation does not affect the instability criterion.

If complex equivalent depths are considered, these conclusions are radically altered. We confine our attention to those eigenmodes that are bounded on the horizontally infinite equatorial beta-plane and bounded with height. In addition, we require the unstable eigenfunctions to be limited to a pre-assigned horizontal length scale L which is defined by the shear region. Depending on the length scale L, the maximum instability can now occur at a finite rather than infinitessimal vertical scale. Modes with n>0 can now be more unstable than the n = 0 mode. With $L \gtrsim 500$ km, greatest instability occurs when the real and imaginary parts of $\sqrt{gh}$ are the same order of magnitude. The (inviscid) growth rate can now exceed the shear. The eigensolutions are trapped vertically and exhibit poleward and downward phase propagation.

Many recent studies have been undertaken which investigate the effect of mean zonal flow on tropical waves and instabilities. A consequence of the present analysis is that a stationary, non-dissipative

basic state flow with horizontal shear at the equator is inappropriate because it is not a stable solution of the symmetric governing equations. This instability tends to symmetrize the zonal flow with respect to the equator if mechanical dissipation is not too great. It also provides a possible theoretical mechanism for the symmetric component of the 40-50 day oscillation in the tropical atmosphere. While Dunkerton (1981) focused on the ramifications for the middle atmosphere, this study applies the results primarily to tropospheric and oceanic circulations.

References

Anderson, J.R., and R.D. Rosen, 1982: The latitude-height structure of 40-50 day variations in atmospheric angular momentum. Submitted to J. Atmos. Sci.

Boyd, J.P., 1978a: The effects of latitudinal shear on equatorial waves. Part I: Theory and Methods. J. Atmos. Sci., 35, 2236-2258.

Boyd, J.P., 1978b: The effects of latitudinal shear on equatorial waves. Part II: Applications to the atmosphere. J. Atmos. Sci., 35, 2259-2267.

Boyd, J.P., and Z.D. Christidis, 1982: Low wavenumber instability on the equatorial beta-plane. Geophys. Res. Lett., 769-772.

Charney, J.G., 1973: Planetary fluid dynamics. Dynamic Meteorology, edited by P. Morel. D. Reidel Publishing Company. 622 pp.

Dunkerton, T., J. 1981: On the inertial stability of the equatorial middle atmosphere. J. Atmos. Sci., 38, 2354-2365.

Dunkerton, T.J., 1982a: Curvature diminution in equatorial wave, mean-flow interaction. J. Atmos. Sci., 39, 182-186.

Dunkerton, T.J., 1982b: A nonsymmetric equatorial inertial instability. Submitted to J. Atmos. Sci.

Eliassen, A., 1952: Slow thermally or frictionally controlled meridional circulation in a circular vortex. Astrophys. Norv., 5, No. 2, 60 pp.

Hayashi, Y. 1970: A theory of large-scale equatorial waves generated by condensation heat and accelerating the zonal wind. J. Meteor. Soc. Japan, 48, 140-160.

Held, I.M., and A.Y. Hou, 1980: Nonlinear axially symmetric circulations in a nearly inviscid atmosphere. J. Atmos. Sci., 37, 515-533.

Hisard, P., J. Merle, and B. Voituriez, 1970: The Equatorial Undercurrent at 170°E in March and April 1967. J. Mar. Res., 28, 281-303.

Holton, J.R., 1979: Equatorial wave-mean flow interaction: A numerical study of the role of latitudinal shear. J. Atmos. Sci., 36, 1030-1040.

Hoskins, B.J., 1974: The role of potential vorticity in symmetric stability and instability. Quart. J. Roy. Met. Soc., 100, 480-482.

Krishnamurti, T.N., 1982: Low-frequency modes in the tropics. Paper 4.18 presented at 14th Technical Conference on Hurricanes and Tropical Meteorology of the AMS, June 7-11, San Diego, CA.

Lindzen, R.S., 1967: Planetary waves on beta-planes. Mon. Wea. Rev., 95, 441-451.

Lindzen, R.S., 1974: Wave-CISK in the tropics. J. Atmos. Sci., 31, 156-179.

Madden, R.A., and P.R. Julian, 1971: Detection of a 40-50 day oscillation in the zonal wind in the tropical Pacific. J. Atmos. Sci., 28, 702-708.

Matsuno, T., 1966: Quasi-geostrophic motions in the equatorial area. J. Met. Soc. Japan, 44, 25-43.

McPhaden, M.J., and R.A. Knox, 1979: Equatorial Kelvin and inertio-gravity waves in zonal shear flow. J. Phys. Ocean., 9, 263-277.

McPhaden, M.J., 1981: Continuously stratified models of the steady equatorial ocean. J. Phys. Ocean., 11, 337-354.

Newell, R.E., J.W. Kidson, D.G. Vincent, and G.J. Boer, 1974: The General Circulation of the Tropical Atmosphere and Interactions with Extratropical Latitudes, Vol. II. The M.I.T. Press, 371 pp.

Ooyama, K., 1969: Numerical simulation of the life cycle of tropical cyclones. J. Atmos. Sci., 26, 3-40.

Philander, S.G.H., 1978: Instabilities of zonal equatorial currents, 2. J. Geophys. Res., 81, 3679-3682.

Philander, S.G.H., 1979: Equatorial waves in the presence of the equatorial undercurrent. J. Phys. Ocean., 9, 254-262.

Phillips, N.A., 1966: The equations of motion for a shallow rotating atmosphere and the "Traditional Approximation." J. Atmos. Sci., 23, 626-628.

Schubert, W.H., and J.J. Hack, 1982: Inertial stability and tropical cyclone development. Submitted to J. Atmos. Sci.

Shapiro, L.J., and H.E. Willoughby, 1982: The response of balanced hurricanes to local sources of heat and momentum. J. Atmos. Sci., 39, 378-394.

Stevens, D.E. and R.S. Lindzen, 1978: Tropical wave-CISK with a moisture budget and cumulus friction. J. Atmos. Sci., 35, 940-961.

n	L (km)	c_s (ms^{-1})	$c_{r,max}$ (ms^{-1})	$c_{i,max}$ (ms^{-1})				
				c_r=0.01	c_r=0.1	c_r=1	c_r=10	c_r=100 ms^{-1}
0	100	0.229	0.229	0.0468	0.114	---	---	---
	300	2.06	2.06	0.143	0.443	1.03	---	---
	1000	22.9	22.9	0.478	1.51	4.68	11.4	---
	3000	206.	206.	1.44	4.54	14.3	44.3	103.
2	100	0.229	0.0458	0.0189	---	---	---	---
	300	2.06	0.412	0.0634	0.177	---	---	---
	1000	22.9	4.58	0.214	0.669	1.89	---	---
	3000	206.	41.2	0.642	2.03	6.34	17.7	---
4	100	0.229	0.0254	0.0124	---	---	---	---
	300	2.06	0.229	0.0468	0.114	---	---	---
	1000	22.9	2.54	0.159	0.494	1.24	---	---
	3000	206.	22.9	0.478	1.51	4.68	11.4	---

Table 1: Maximum c_r and c_i for several values of n and L. Linear shear ($\delta = 0$) is assumed.

L (km)	σ_r ($10^{-5}s^{-1}$)	σ_i ($10^{-5}s^{-1}$)	λ_r	λ_i	c_r (ms^{-1})	c_i (ms^{-1})
300	0.0344	0.499	-47.4	711	0.01	0.15
1000	1.6	0.8	-4	5	10	11
3000	5.2	2.2	-0.4	0.7	100	100

Table 2: Characteristics of most unstable modes with L = 300, 1000, 3000 km. n = 0.

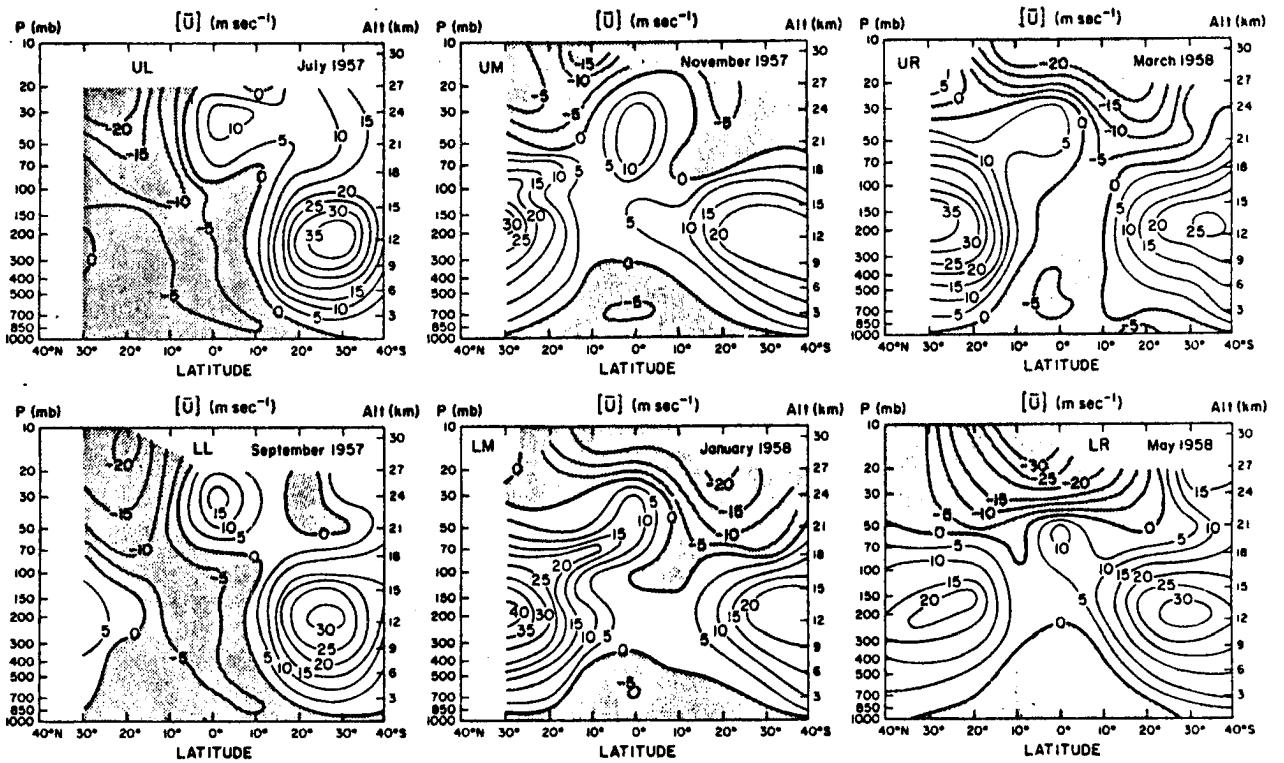

Figure 1: Atmospheric mean zonal wind (m s^{-1}) at 2-month intervals (after Boyd, 1978b, and Newell et al., 1974).

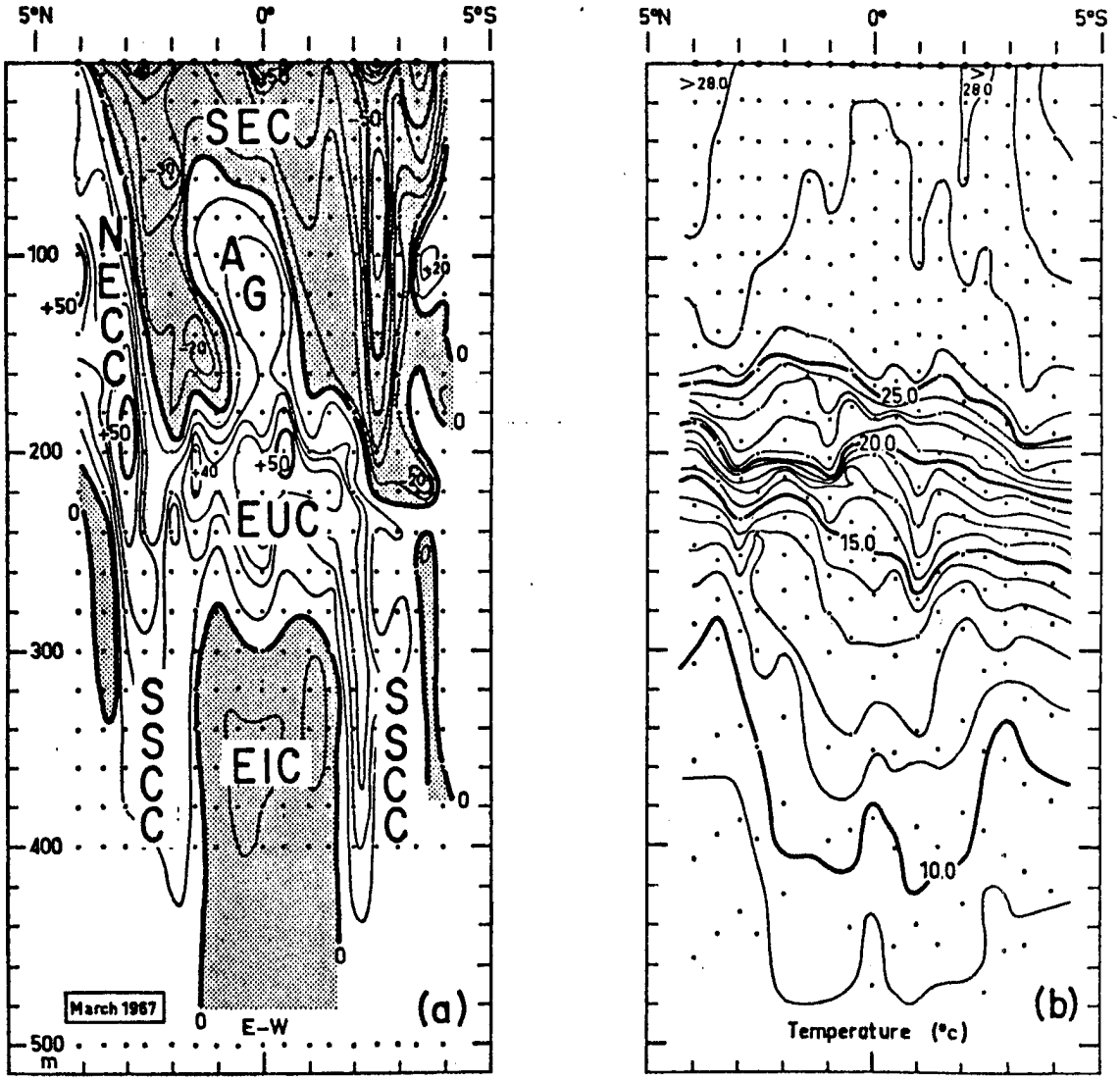

Figure 2: (a) Meridional section of zonal velocity (cm s^{-1}) at 170°E in the uppermost 500 m of the Pacific Ocean. Regions of easterly flow are stippled. (b) Corresponding meridional section of temperature (°C) (after McPhaden, 1981, and Hisard, et al., 1970).

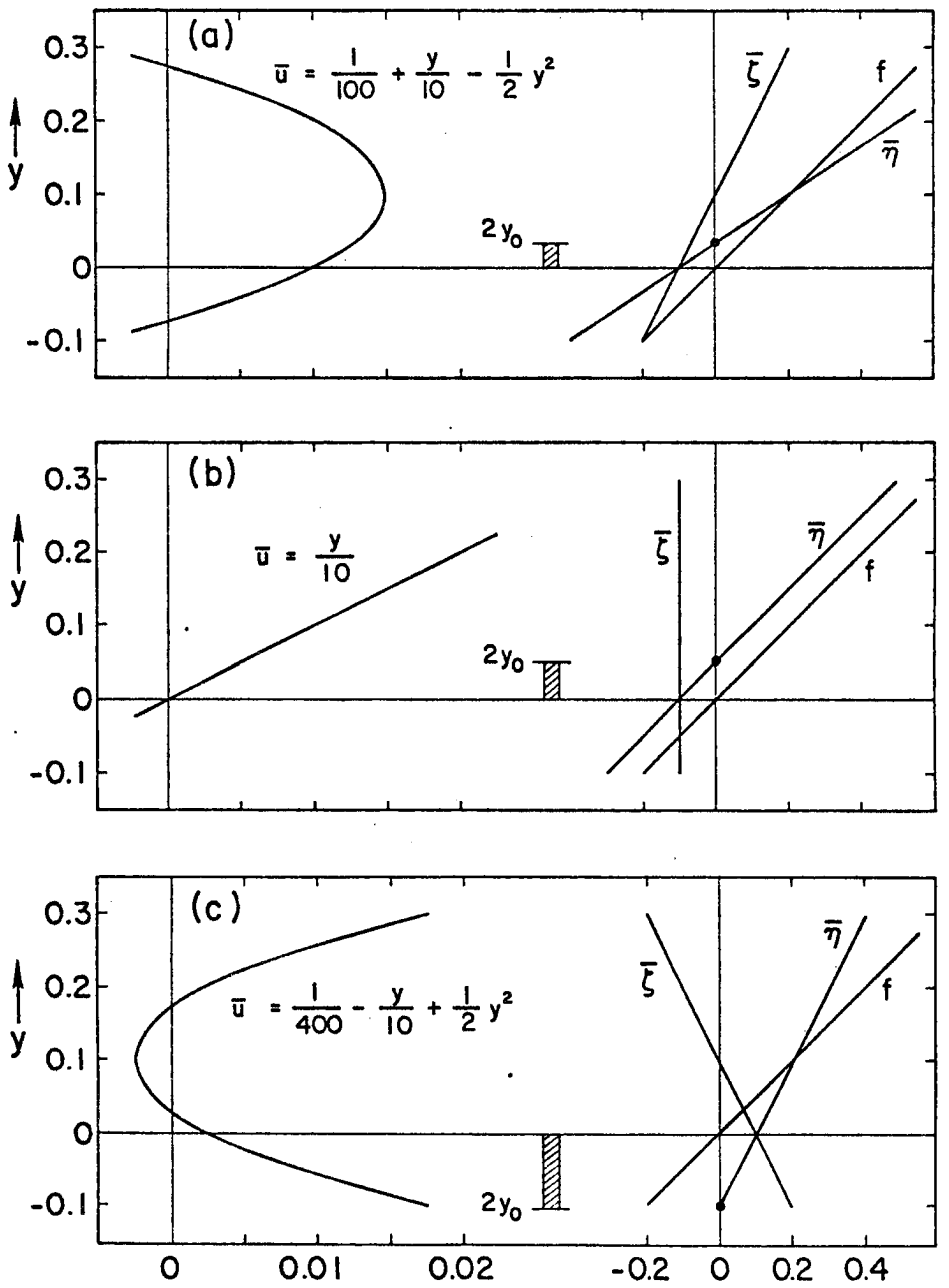

Figure 3: Typical flow geometries for (a) a westerly jet ($U_o = 0.01$, $\gamma = 0.1$, $\delta = -1$); (b) linear shear flow ($U_o = 0$, $\gamma = 0.1$, $\delta = 0$); (c) an easterly jet ($U_o = 0.025$, $\gamma = -0.1$, $\delta = 1$). For illustrative purposes, y is non-dimensionalized by a, $\bar{U}$ and U_o by Ωa, and f, $\bar{\zeta}$, and $\bar{\eta}$ by Ω. Non-dimensional $\beta = 2$.

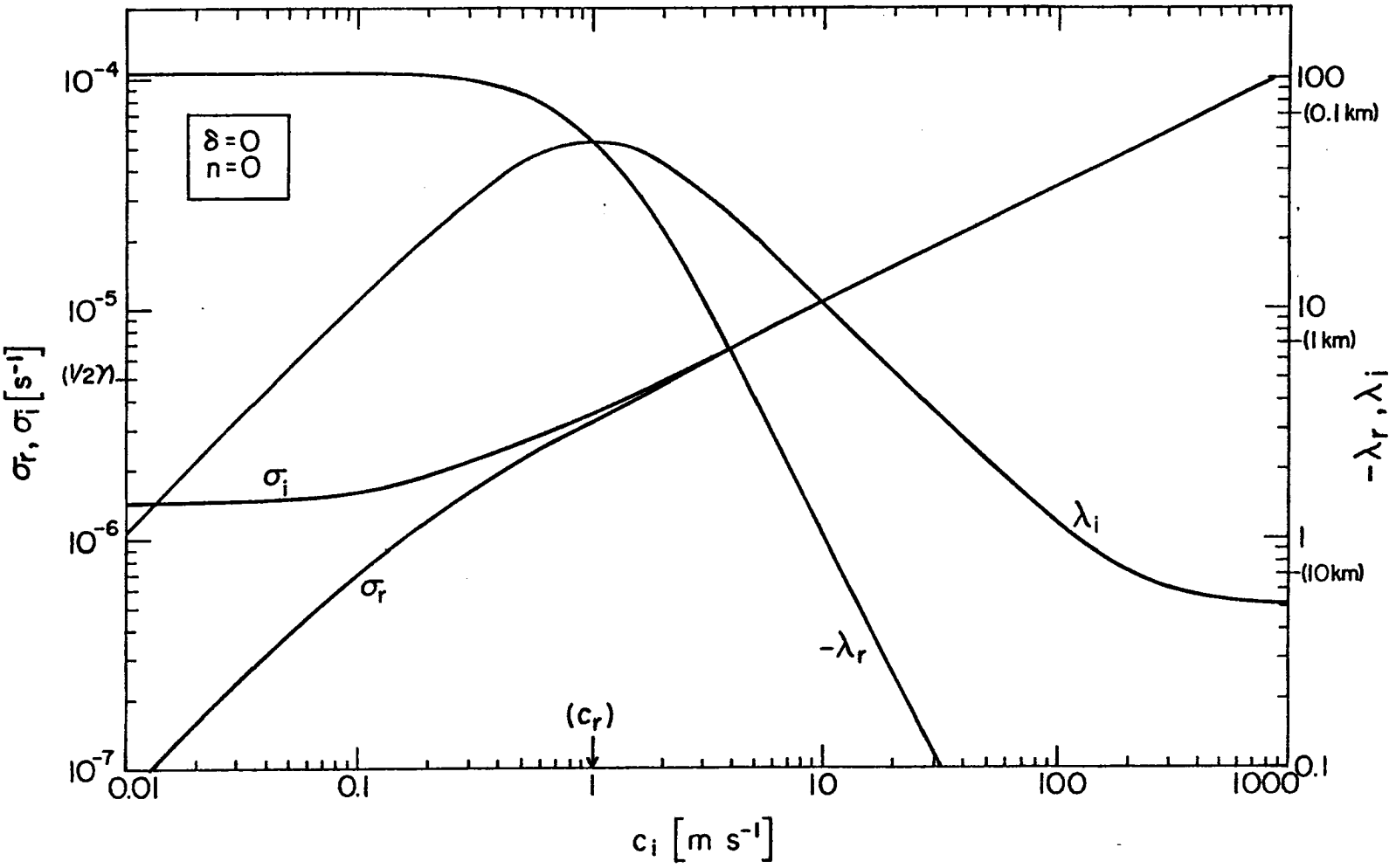

Figure 4: Real (σ_r) and imaginary (σ_i) parts of complex frequency, and negative real ($-\lambda_r$) and imaginary (λ_i) parts of complex vertical wavenumber; as a function of c_i, with $c_r = 1\ ms^{-1}$, $\gamma = 10^{-5}s^{-1}$, $\delta = 0$, $n = 0$. On the right is the dimensional scale corresponding to λ, with an assumed 7 km scale height.

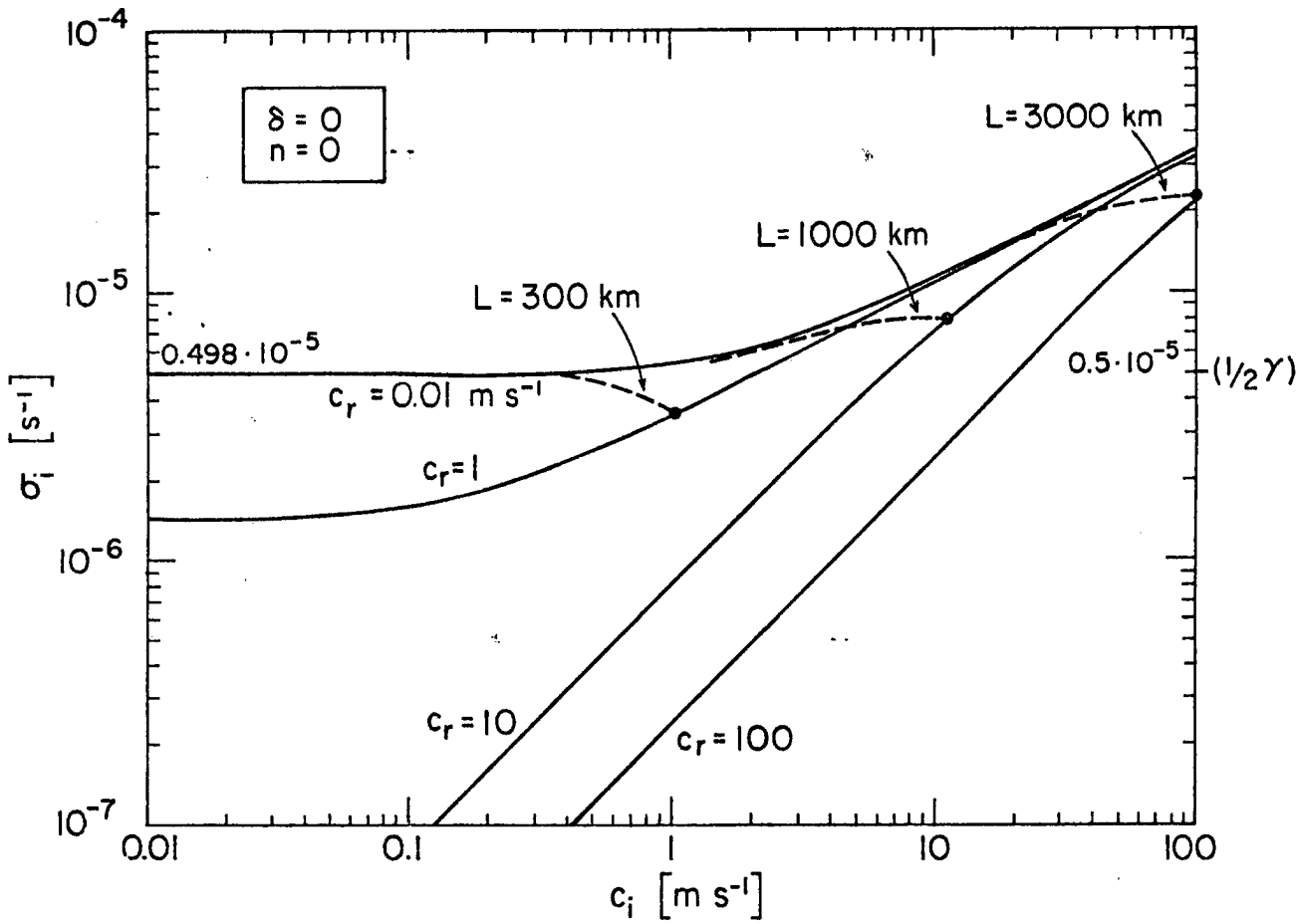

Figure 5: Growth rate (σ_i) as a function of c_i for c_r = 0.01, 1, 10, 100 ms^{-1}. $\gamma = 10^{-5} s^{-1}$, $\delta = 0$, $n = 0$. Maximum growth rate with real c is ½ γ. Dashed curves show the limits on growth rate for L = 300, 1000, 3000 km.

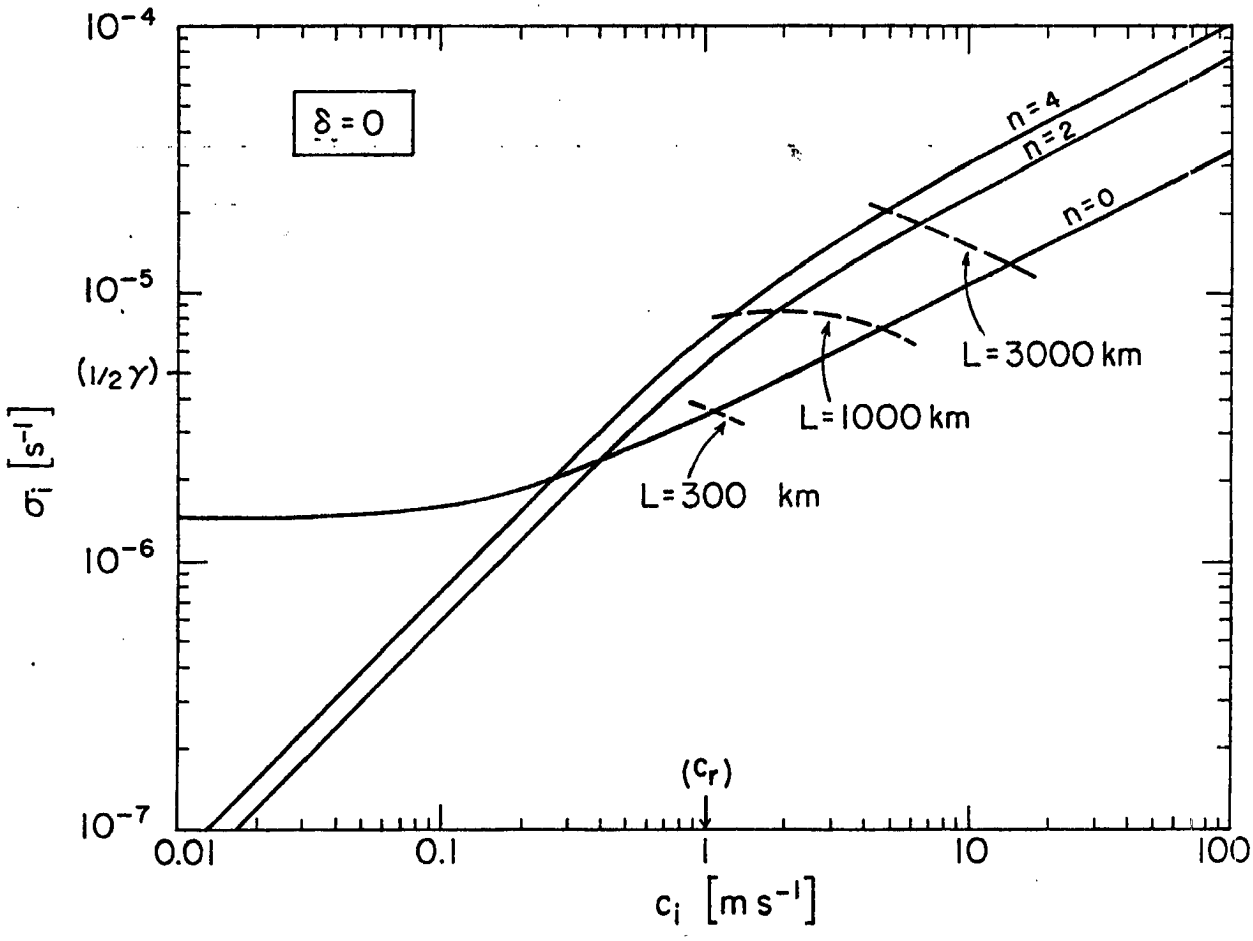

Figure 6: Growth rate (σ_i) as a function of c_i for c_r = 1 ms^{-1} and n = 0, 2, 4. $\gamma = 10^{-5} s^{-1}$, $\delta = 0$. Maximum growth rate with real c is ½ γ. Dashed curves show the limits on growth rate for L = 300, 1000, 3000 km.

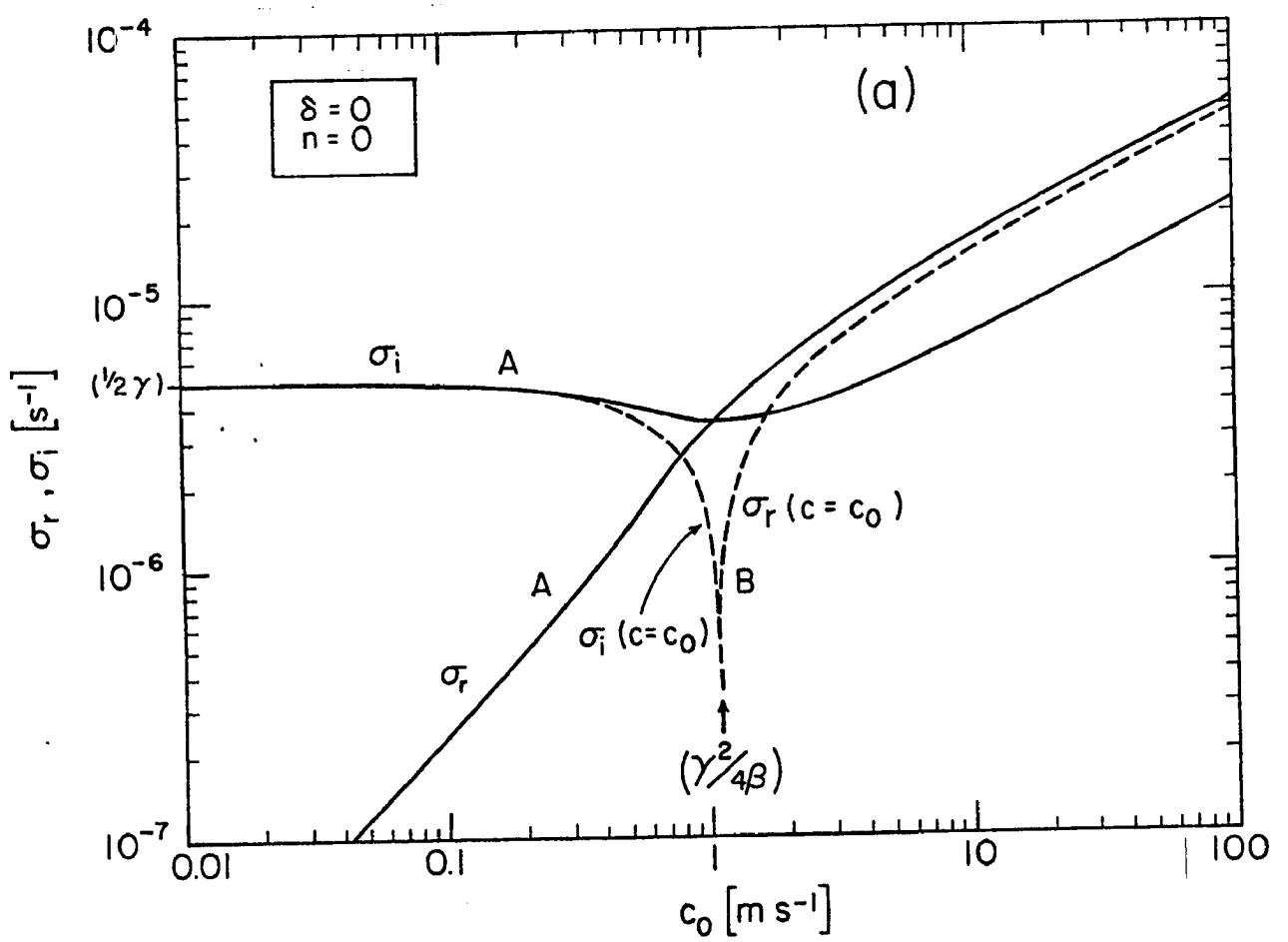

Figure 7: (a) Growth rate (σ_i) and frequency (σ_r) for two cases: (A) $c_r = c_i = c_o$ (solid) and (B) $c = c_r = c_o$ (dashed). $n = 0$, $\delta = 0$, $\gamma = 10^{-5} s^{-1}$.

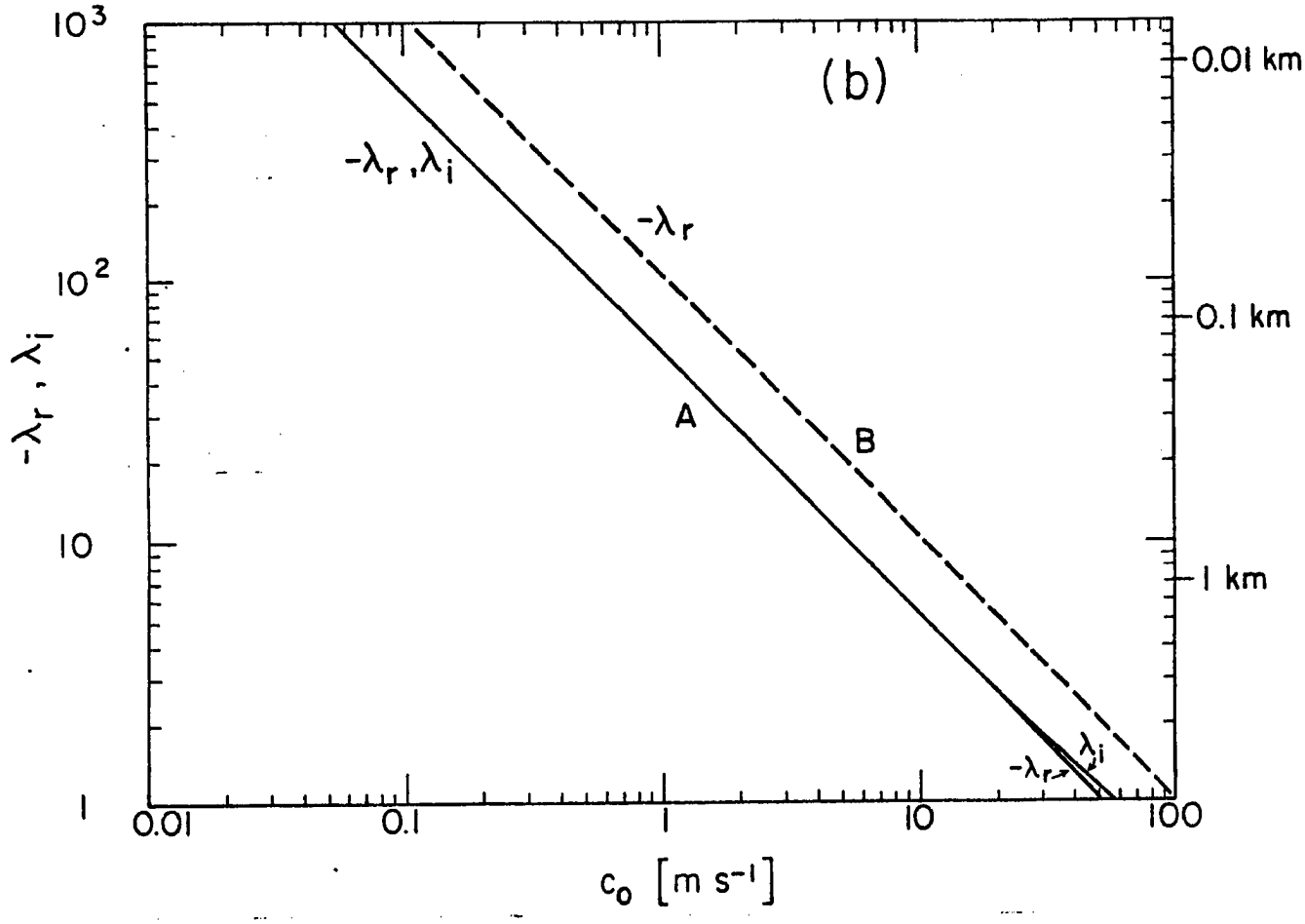

Figure 7: (b) Negative real component ($-\lambda_r$) and imaginary component (λ_i) of the vertical wavenumber for case A (solid) and case B (dashed). $\lambda_i = 0$ in case B for $c_o < (4R\Gamma)^{\frac{1}{2}} = 214$ ms^{-1}.

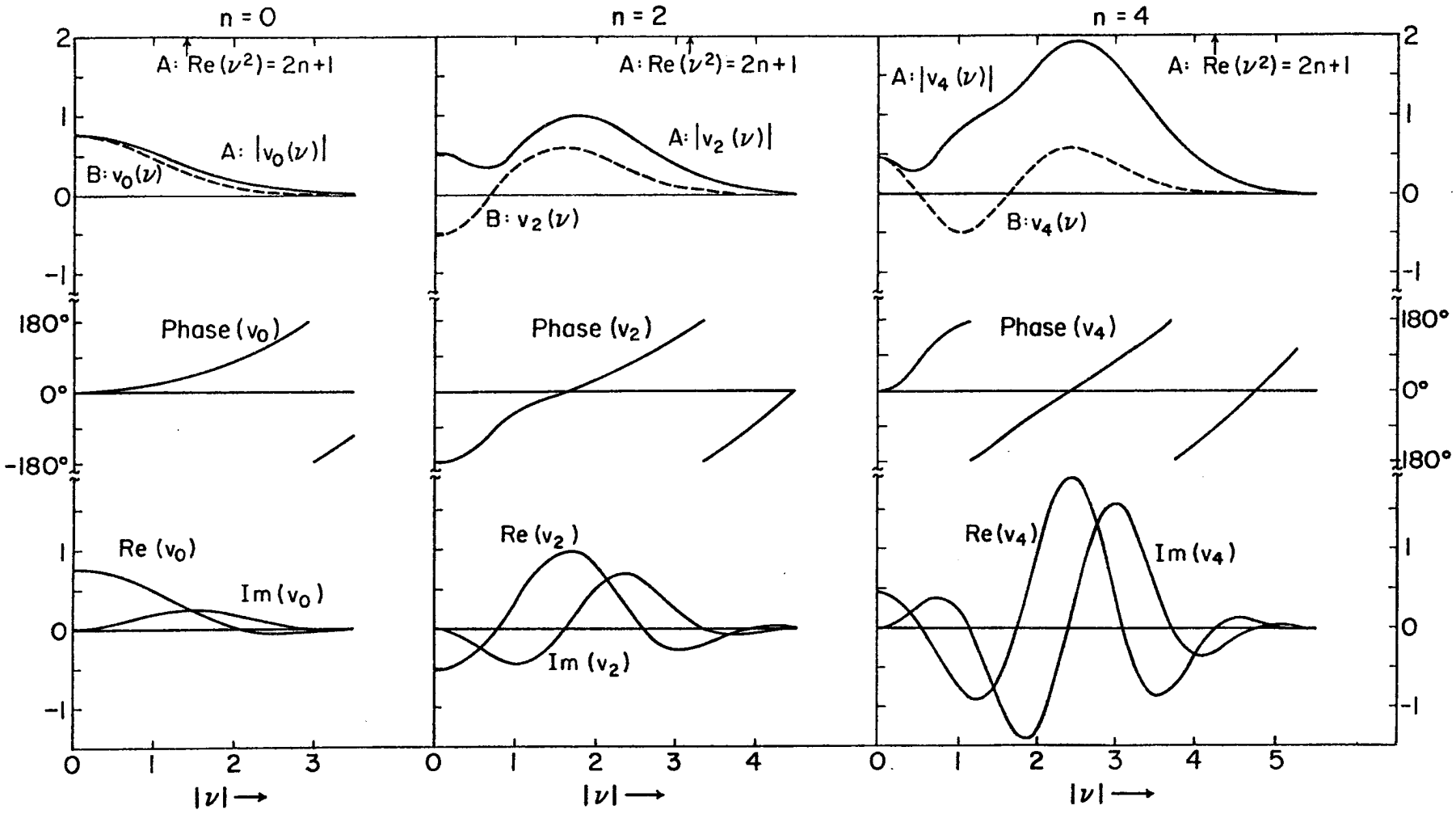

Figure 8: $v_n(\nu)$ of (3.15) for n = 0, 2, 4.
Case A (solid): $c_r = c_i = c_o$ -- complex separation constant.
Case B (dashed): $c = c_r = c_o$ -- real separation constant.
$v_n(\nu)$ is normalized so that $\int_{-\infty}^{\infty} v_n^2 d\nu = 1$.

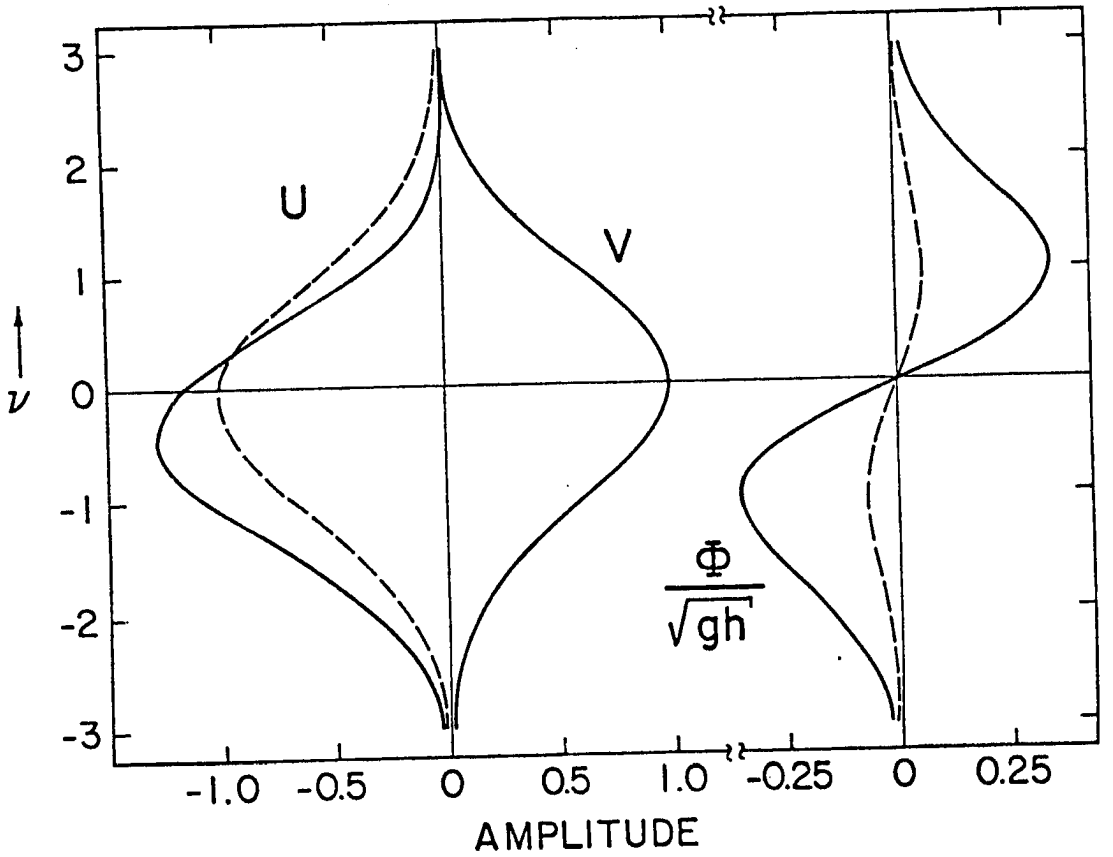

Figure 9: Horizontal structure of u, v, $\Phi/\sqrt{gh}$ as a function of ν for the n = 0 mode in linear shear flow. Arbitrary constant (C_n) in (3.15) is unity. Solid lines represent $\xi_o = 2$ case; dashed lines represent u, $\Phi/\sqrt{gh}$ fields for $\xi_o = 10$ case.

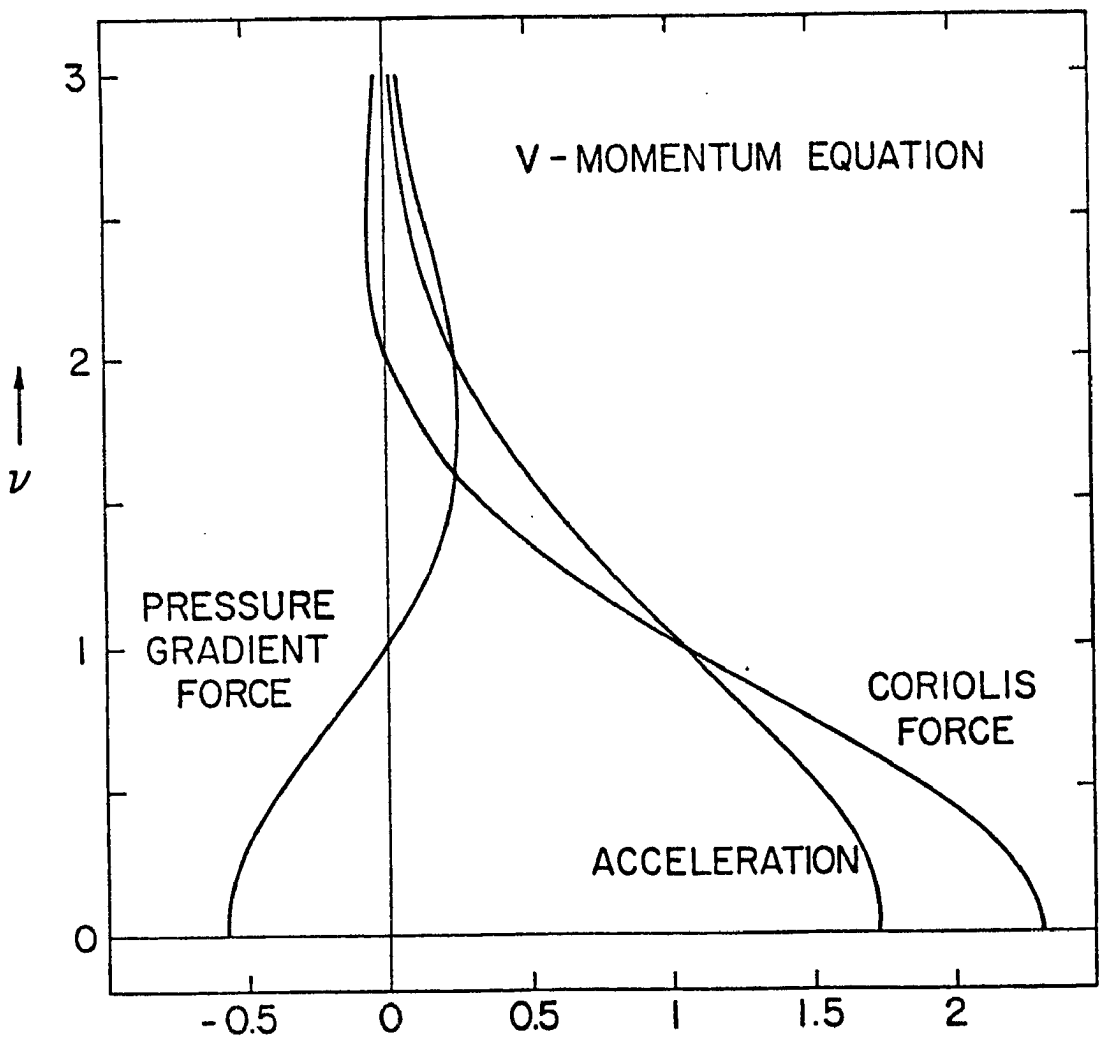

Figure 10: Balance of forces in v-momentum equation. Arbitrary constant (C_n) in (3.15) is unity. $\xi_o = 2$, $\delta = 0$.

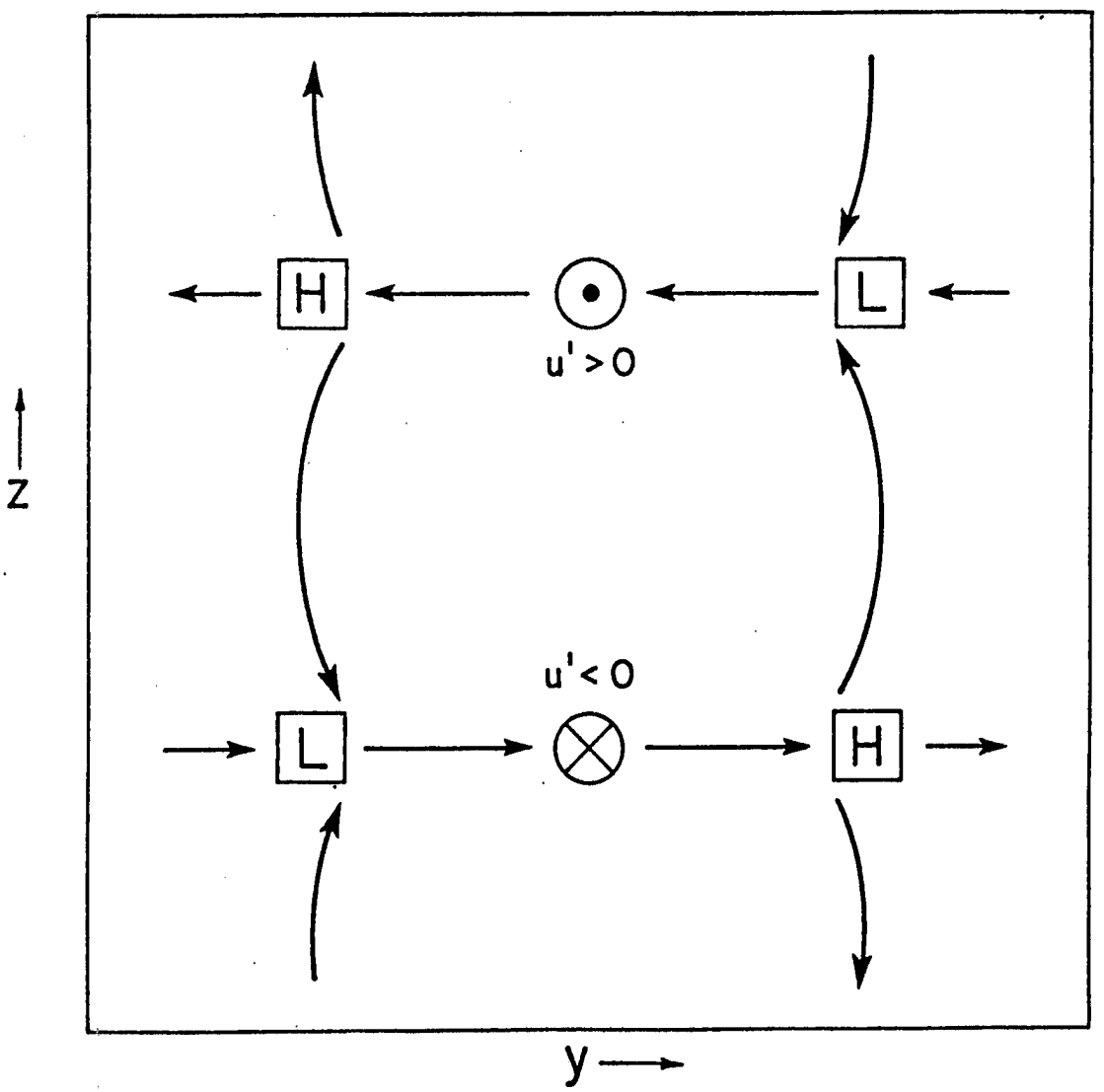

Figure 11: Schematic illustration of the structure of the instability in the meridional plane. L and H indicate regions of low pressure and high pressure, respectively.